

# Accessory and rock forming minerals monitoring the evolution of zoned mafic–ultramafic complexes in the Central Ural Mountains

J. Krause <sup>a,b,\*</sup>, G.E. Brügmann <sup>b</sup>, E.V. Pushkarev <sup>c</sup>

<sup>a</sup> *Institut für Geowissenschaften, Universität Mainz, Becherweg 21, D-55099 Mainz, Germany*

<sup>b</sup> *Max-Planck-Institut für Chemie, Becherweg 27, D-55020 Mainz, Germany*

<sup>c</sup> *Institute of Geology and Geochemistry, Russ. Acad. Sciences, 620151 Ekaterinburg, Russia*

Received 5 December 2005; accepted 15 July 2006

Available online 4 October 2006

## Abstract

This study describes major and trace element compositions of accessory and rock forming minerals from three Uralian–Alaskan-type complexes in the Ural Mountains (Kytlym, Svetley Bor, Nizhnii Tagil) for the purpose of constraining the origin, evolution and composition of their parental melts. The mafic–ultramafic complexes in the Urals are aligned along a narrow, 900 km long belt. They consist of a central dunite body grading outward into clinopyroxenite and gabbro lithologies. Several of these dunite bodies have chromitites with platinum group element mineralization.

High Fo contents in olivine (Fo 92–93) and high Cr/(Cr+Al) in spinel (0.67–0.84) suggest a MgO-rich (>15 wt.%) and Al<sub>2</sub>O<sub>3</sub>-poor ultramafic parental magma. During its early stages the magma crystallized dominantly olivine, spinel and clinopyroxene forming cumulates of dunite, wehrlite and clinopyroxenite. This stage is monitored by a common decrease in the MgO content in olivine (Fo 93–86) and the Cr/(Cr+Al) value of coexisting accessory chromite (0.81–0.70). Subsequently, at subsolidus conditions, the chromite equilibrated with the surrounding silicates producing Fe-rich spinel while Al-rich spinel exsolved chromian picotite and chromian titanomagnetite. This generated the wide compositional ranges typical for spinel from Uralian–Alaskan-type complexes world wide.

Laser ablation analyses (LA-ICPMS) reveal that clinopyroxene from dunites and clinopyroxenite from all three complexes have similar REE patterns with an enrichment of LREE (0.5–5.2 prim. mantle) and other highly incompatible elements (U, Th, Ba, Rb) relative to the HREE (0.25–2.0 prim. mantle). This large concentration range implies the extensive crystallization of olivine and clinopyroxene together with spinel from a continuously replenished, tapped and crystallizing magma chamber. Final crystallization of the melt in the pore spaces of the cooling cumulate pile explains the large variation in REE concentrations on the scale of a thin section, the REE-rich rims on zoned clinopyroxene phenocrysts (e.g. La<sub>Rim</sub>/La<sub>Core</sub> ~ 2), and the formation of interstitial clinopyroxene with similar REE enrichment.

Trace element patterns of the parental melt inferred from clinopyroxene analyses show negative anomalies for Ti, Zr, Hf, and a positive anomaly for Sr. These imply a subduction related geotectonic setting for the Uralian zoned mafic–ultramafic complexes. Ankaramites share many petrological and geochemical features with these complexes and could represent the parental melts of this class of mafic–ultramafic intrusions.

Diopside from chromitites and cross cutting diopside veins in dunite has similar trace element patterns with LREE/HREE ratios (e.g. La/Lu=5–60) much higher than those in diopside from all other lithologies. We suggest that the chromitites formed at high

\* Corresponding author. Institut für Geowissenschaften, Universität Mainz, Becherweg 21, D-55099 Mainz, Germany. Fax: +49 6131 371051.  
E-mail address: [krause@mpch-mainz.mpg.de](mailto:krause@mpch-mainz.mpg.de) (J. Krause).

temperatures (800–900 °C) during the waning stages of solidification as a result of the interaction of an incompatible element-rich melt or fluid with the dunite cumulates.

© 2006 Elsevier B.V. All rights reserved.

*Keywords:* Uralian–Alaskan-type complex; Ural Mountains; Spinel; Chromitite; Parental melt; Ankaramites

## 1. Introduction

Uralian–Alaskan-type zoned mafic–ultramafic complexes are a class of intrusions which are distinct with regard to their tectonic setting, internal structure and petrology (Taylor and Noble, 1960; Noble and Taylor, 1960; Himmelberg et al., 1986; Himmelberg and Loney, 1995). The complexes are known from convergent margin settings, for example the Ural Mountains (Noble and Taylor, 1960; Taylor, 1967), the Cordillera of Alaska and British Columbia (Findlay, 1969; Clark, 1980; Himmelberg et al., 1986; Nixon et al., 1990; Himmelberg and Loney, 1995), and on Northern Kamchatka, Russia (Batanova and Astrakhtantsev, 1992; Batanova and Astrakhtantsev, 1994). The intrusions are distributed along narrow belts often several hundreds of kilometres long. Their classical distinctive geologic and petrographic feature is a zonal distribution of mafic and ultramafic rocks. Often a central dunite body grades outward into wehrlite, clinopyroxenite and gabbroic lithologies. Many of these complexes host a mineralization of platinum group minerals (PGM) locally of economic importance.

In the Ural Mountains 15 Uralian–Alaskan-type mafic–ultramafic complexes define a linear belt along the 60-th meridian, which is about 900 km long (Fig. 1a). Due to the occurrence of economic platinum deposits associated with these complexes this chain is called the “Ural platinum belt” (UPB). This is a narrow belt in the middle and southern part of the Tagil–Magnitogorsk zone consisting of island arc related volcanic rocks and plutons in tectonic contact with ophiolite fragments and different types of mafic to ultramafic intrusive complexes.

For the Uralian–Alaskan-type complexes of the UPB important geological and geochemical features such as the age and mechanism of emplacement or the composition and evolution of their parental melts are poorly understood. In addition the origin of the chromitites, sources for PGM placer deposits, is not well known.

The composition of minerals, rock forming and accessory phases, is controlled by parameters such as pressure, temperature and the composition of the parental magma. This is why the chemical composition of minerals, such as chromian spinel, give important information regarding the degree of partial melting in

the mantle or the evolution of mantle melts during their rise to the surface (e.g. Hill and Roeder, 1974; Sack and Ghiorso, 1991a,b; Van der Veen and Maaskant, 1995). The compositional variations of chromian spinel can be further used to discriminate among different tectonic settings (e.g. Irvine, 1967; Roeder, 1994; Cookenboo et al., 1997; Zhou et al., 1997; Lee, 1999; Barnes and Roeder, 2001). However, one has to keep in mind that the composition of chromian spinel can be easily re-equilibrated at subsolidus conditions.

Trace element concentrations, for example those of the REE, play a key role in monitoring the fractionation of silicate melts. In particular in cumulate rocks, where there is no direct access to the melt composition, the trace element distribution in minerals provides powerful clues to the origin and evolution of the parental melts. For example, melt compositions can be calculated with experimentally determined mineral–melt partition coefficients and calculated trace element patterns can be compared with those of natural samples from different tectonic environments (e.g. McKenzie and O’Nions, 1991; Hart and Dunn, 1993; Ionov et al., 1997; Bédard, 2001; Ionov et al., 2002).

In this study we present new major and trace element data from rocks and minerals from three Uralian–Alaskan-type complexes in the middle and southern Urals. The comparison of the chemical composition of olivine and chromian spinel from the Urals with data from other localities indicates that they are unique intrusions having a characteristic spinel chemistry. Laser-ICPMS analyses of trace element concentrations in clinopyroxene are used to calculate the melt composition. The mineral compositions monitor the evolution of the parental magmas and decipher differences between the complexes. The data also show that ankaramites could be the parental magmas of Uralian–Alaskan-type complexes.

## 2. Samples and analytical methods

### 2.1. Sample description

For this study dunites, chromitites, wehrlites, clinopyroxenites, hornblendites and gabbros were sampled from three Uralian–Alaskan-type complexes of the UPB.

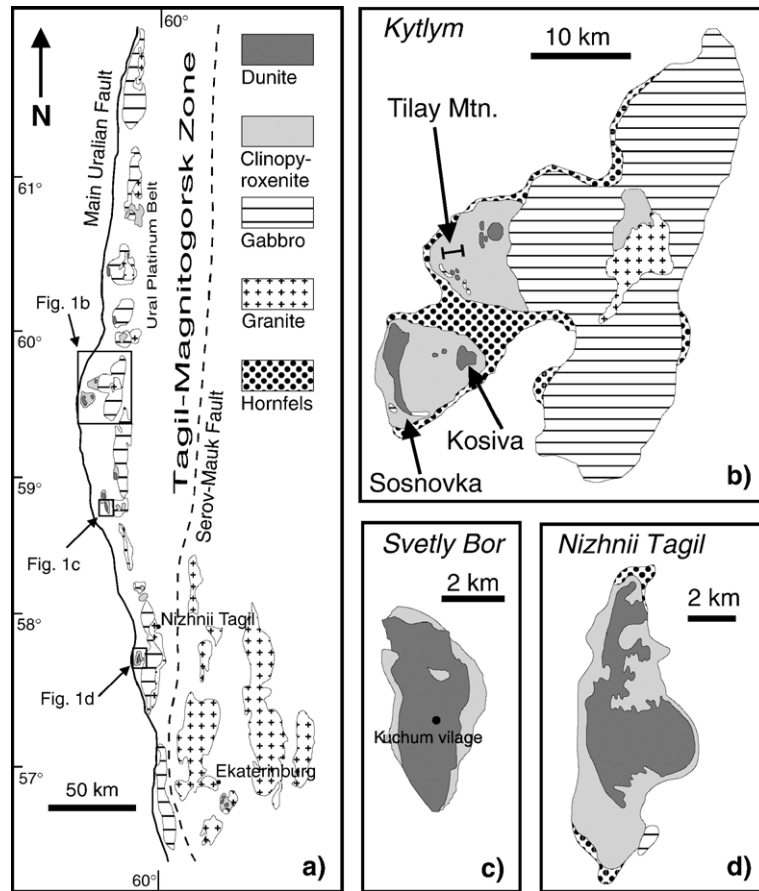


Fig. 1. Geological maps of the Ural platinum belt (a) and the studied Uralian–Alaskan-type complexes (b–d). Modified after Chashchukhin et al. (2002) and Garuti et al. (1997).

The Nizhnii Tagil complex is dominated by dunite of different grain sizes and textures containing chromitites in places (Fig. 1d) (Chashchukhin et al., 2002; Savelieva et al., 2002). The dunites are overlain by clinopyroxenites with, in places, a few meters of wehrlite at the contact. Gabbro occurs only in a small body at the south-eastern rim of the complex.

In the dunitic core of the Svetley Bor complex no chromitites have been found (Fig. 1c). This core is surrounded by clinopyroxenite that locally contains hornblendites. Gabbroic rocks are not exposed in this complex (Garuti et al., 1997).

The Kytlym complex is the largest of the studied complexes (Fig. 1b). Several dunite bodies (Sosnovka, Kosiva Mountain, Tilay Mountain) are surrounded by clinopyroxenite. Some of the dunite bodies contain chromitites. Several smaller and at least two larger gabbro massifs are also present (Garuti et al., 1997; Savelieva et al., 1999, 2002; Chashchukhin et al., 2002). In places tectonically induced interlayering between different

lithologies can be observed. Lithological contacts are sharp and a foliation is often visible.

Dunites consist of 97–99% olivine, and up to 2% of accessory chromite. Interstitial clinopyroxene is present in most of the samples as an accessory component. Amphibole was found in one, strongly serpentinized sample. The degree of serpentinization is variable (5–50%) and often is extensive if the rocks are foliated. Dunites from each complex are crosscut by millimetre to centimetre wide, coarse grained (up to 1 cm grain size) clinopyroxenite veins consisting of pure, green diopside. Dykes of hornblendite, centimetre to decimetre wide, occur in the dunite bodies of the Svetley Bor and the Sosnovka dunite (Kytlym).

Chromitites occur as lenses several millimetres to decimetres in size and consist of more than 80% chromite. Relict olivine and clinopyroxene as well as serpentine, talc, chlorite and other retrograde minerals are present along chromite grain boundaries as well as crosscutting cracks in the chromitite. Sulphides such as pentlandite and

platinum group minerals such as isoferroplatinum and tetraferroplatinum occur as idiomorphic grains either included in the chromite or along grain boundaries. Most of the chromitites are surrounded by a millimetre thick green serpentine rim at the contact to the dunite. According to Chashchukhin et al. (2002) the occurrence of chromitite lenses and schlieren is accompanied by a recrystallization of olivine in the neighbouring dunite.

The clinopyroxenites consist of 90 to 99% clinopyroxene with minor amounts of olivine and hornblende. Spinel, apatite, titanite and sulphides are accessory phases. The textures vary from equigranular to porphyric. A wehrlite zone several centimetres to metres wide is often present at the contact between the clinopyroxenite and the dunite. An interlayering of clinopyroxenite with hornblendite occurs in several places in Svetley Bor. Here clinopyroxene and hornblende coexist along 0.5 to 1 cm thick bands with equilibrated grain boundaries. This could signify the interaction of a fluid or melt phase with pre-existing clinopyroxenite.

In the Kosiva Mountain area of Kytlym and in Svetley Bor hornblendites form centimetres to decimetres wide dykes crosscutting dunites and clinopyroxenites. However massive bodies of hornblendite to hornblendite–pyroxenites can also be found. Clinopyroxene, in places partially replaced by hornblende, often forms idiomorphic phenocrysts in a hornblende-rich matrix, which also contains accessory phases such as sulphides, spinel, titanite, ilmenite and apatite.

The gabbros consist of 30 to 70% clinopyroxene phenocrysts in a matrix of olivine, phlogopite, plagioclase (bytownite), and pseudoleucite (nepehline-K-feldspar intergrowth). In places with a higher feldspar content the gabbros are often strongly foliated with a protomylonitic texture and sharp tectonic contacts to the clinopyroxenites.

## 2.2. Major element analysis

After removing weathered crusts, the samples were powdered in an agate mill for XRF analysis. Polished thin sections 35 and 150  $\mu\text{m}$  thick were used for the microprobe and Laser-ICPMS measurements. The XRF analyses were conducted with a Philips MagiXPRO spectrometer at the University of Mainz. Minerals were analysed with the Jeol JXA8200 microprobe of the Max-Planck-Institute for Chemistry and the Jeol JXA 8900RL microprobe at the Institute of Geosciences of the University of Mainz. We used natural minerals and oxides (Si, Ti, Al, Fe, Mg, Mn, Ca, Na, K, Cr, Zn) and pure element standards (V, Co) for calibration. Silicate minerals were measured with an acceleration voltage of

15 or 20 kV and a probe current of 12 or 20 nA. For the spinel analysis voltages and currents of 20 kV and 12 or 20 nA were used. Element maps were obtained with a 20 kV and 20 nA electron beam.

## 2.3. Trace element analysis

A New Wave UP213 laser system with a wavelength of 213 nm for the ablation was used to determine the trace element concentrations in clinopyroxene and hornblende. Applying a frequency of 10 Hz and energies between 2 and 12  $\text{J}/\text{cm}^2$  produced ablation pits with diameters of 80 and 120  $\mu\text{m}$ . Helium was used as the carrier gas. The ablated material was analyzed with a ThermoFinnigan Element2 sectorfield ICPMS in the low resolution mode and a measuring time of 20 s on the background and 80 to 100 s on the sample. NIST612, KL2G and GOR132 were used as standard materials. The analytical procedure is described in more detail by Jochum et al. (submitted for publication).

## 3. Results

Due to the large number of analysis (34 whole rock analyses, 584 olivine, 1326 spinel, 892 clinopyroxene with microprobe and 289 trace element analyses of clinopyroxene) only selected analyses can be here presented in Tables 1–4. The entire dataset can be found in the online version.

### 3.1. Major element composition of whole rocks

The major element composition for selected samples is shown in Table 1. There are systematic trends among the major element oxides, e.g.  $\text{Al}_2\text{O}_3$ , CaO, and  $\text{TiO}_2$  with MgO, which are controlled by the lithology of the samples (Fig. 2).

The  $\text{Al}_2\text{O}_3$  content rises from less than 1 wt.% in the dunites and 1.6–3.3 wt.% in the clinopyroxenites to values between 2.0 wt.% and 16.4 wt.% in the hornblendites and gabbros. Most dunites also have low CaO concentrations of less than 1 wt.%, whereas the clinopyroxenites contain the highest CaO concentrations of all rock types (15.5–23.4 wt.%). The CaO decreases slightly in the gabbro (11.5–20.0 wt.%) and the hornblendite (13.7–21.2 wt.%). The  $\text{TiO}_2$  content is lowest in the dunites (0.02–0.04 wt.%), but increases in the clinopyroxenite (0.18–0.72 wt.%) and the gabbro (0.19–0.77 wt.%), and reaches a maximum in the hornblendite (1.05–1.92 wt.%). A typical feature of all lithologies is the high  $\text{CaO}/\text{Al}_2\text{O}_3$  ratio. It varies from 0.5 to 1.6 in the dunite, 0.9–2 in the hornblendite and 0.9–2.8 in

Table 1  
Whole rock major and trace element contents of selected samples from Uralian–Alaskan-type complexes in the Urals

Sample	NT1	NT3	NT8	NT12	NT13	NT14	SB18	SB22	SB23	SB30	KT32	KT37	KT39	KT44	KT46	KT49
Lithology	Du	Du	Gb	Du	Cp	Wh	Du	Cp	Cp	Hb	Du	Du	Cp	Gb	Gb	Cp
SiO <sub>2</sub> (wt.%)	34.95	36.14	47.64	34.74	46.29	44.98	37.45	51.04	50.87	35.5	37.96	37.85	48.72	45.14	46.65	50.17
TiO <sub>2</sub>	0.02	0.02	0.53	0.02	0.41	0.31	0.02	0.36	0.18	1.88	0.03	0.02	0.33	0.55	0.67	0.26
Al <sub>2</sub> O <sub>3</sub>	0.19	0.21	10.3	0.2	2.75	1.96	0.25	3.42	1.62	10.14	0.26	0.27	2.47	5.42	9.39	3.05
Fe <sub>2</sub> O <sub>3</sub>	8.55	8.38	10.6	6.58	12.32	12	9.08	6.22	5.55	20.91	11.66	10.95	9.1	12.82	12.52	7.69
MnO	0.17	0.16	0.19	0.12	0.18	0.2	0.16	0.11	0.12	0.23	0.22	0.19	0.16	0.21	0.21	0.15
MgO	43.05	44.42	13.5	43.67	19.18	20.92	45.78	15.06	19.9	8.44	45.23	45.33	19.61	19.76	12.68	17.3
CaO	0.3	0.3	11.38	0.19	18.19	15.39	0.25	23.16	20.4	20.69	0.32	0.26	19.16	15.71	14.22	19.94
Na <sub>2</sub> O	b.d.	b.d.	2.15	b.d.	0.16	0.03	b.d.	0.15	0.06	0.33	b.d.	b.d.	0.13	0.4	1.79	0.23
K <sub>2</sub> O	b.d.	b.d.	2.86	b.d.	0.01	0.01	b.d.	0.01	0.02	0.15	b.d.	b.d.	0.01	0.05	1.26	0.03
P <sub>2</sub> O <sub>5</sub>	b.d.	b.d.	0.34	b.d.	b.d.	b.d.	b.d.	b.d.	b.d.	1.49	b.d.	b.d.	b.d.	0.01	0.24	b.d.
Cr <sub>2</sub> O <sub>3</sub>	0.27	0.39	0.09	0.39	0.14	0.17	0.63	0.06	0.19	0.01	0.57	0.35	0.32	0.17	0.08	0.22
NiO	0.15	0.12	0.03	0.21	0.03	0.03	0.19	0.01	0.03	0.01	0.15	0.16	0.02	0.04	0.02	0.02
LOI	13.42	10.23	0.54	14.54	0.59	4.67	6.6	0.31	1.32	0.41	4.46	5.32	0.44	0.06	0.12	1.23
Total	101.02	100.33	100.15	100.60	100.24	100.67	100.36	99.90	100.26	100.19	100.79	100.66	100.47	100.33	99.85	100.29
CaO/Al <sub>2</sub> O <sub>3</sub>	1.58	1.43	1.10	0.95	6.61	7.85	1.00	6.77	12.59	2.04	1.23	0.96	7.76	2.90	1.51	6.54
Rb (ppm)	2	3	55	2	3	2	4	3	1	5	3	3	2	4	21	2
Sr	6	3	982	4	174	98	7	56	95	200	4	4	80	294	898	76
Ba	16	23	619	15	22	14	20	26	34	b.d.	20	23	20	16	185	58
Sc	3	4	38	3	89	65	3	135	88	76	2	1	78	63	45	89
V	5	6	244	4	179	121	9	188	69	662	9	12	132	229	280	154
Co	126	121	55	111	69	85	131	31	46	60	147	147	57	74	56	53
Cu	b.d.	b.d.	94	b.d.	6	4	b.d.	6	3	17	b.d.	b.d.	7	11	77	10
Zn	45	44	76	34	51	54	48	22	27	98	68	61	42	72	86	36
Y	3	3	14	3	7	6	2	9	6	26	4	3	8	14	14	7
Zr	17	17	54	18	24	20	17	22	20	73	17	17	23	39	55	21

Fe<sub>2</sub>O<sub>3</sub>\* = total iron content NT = Nizhnii Tagil, KT = Kytlym, SB = Svetley Bor, Du = Dunite, Wh = Wehrlite, Cp = Clinopyroxenite, Gb = Gabbro, Hb = Hornblendite, b.d. = below limit of detection.

Table 2  
Olivine compositions of selected samples from Uralian–Alaskan-type intrusions

Sample	NT1-42	NT2-58	NT3-38	NT4-177	NT5-103	NT5-177	NT6-75	NT7-13	NT8-91	NT9a-43	NT12-132	NT13-112	NT15-121	SB16-73	SB18-47
Lithology	Du	Du	Du	Du	Ch*	Ch	Du	Du	Gb	Gb	Du	Wh	Du	Du	Du
SiO <sub>2</sub> (wt.%)	41.28	40.62	40.74	40.74	41.04	40.39	40.28	40.64	38.55	38.36	40.74	39.23	40.64	39.85	40.22
TiO <sub>2</sub>	0.01	0.02	0.02	0.02	0.03	0.02	0.04	b.d.	0.03	b.d.	0.02	0.02	0.02	b.d.	0.01
Al <sub>2</sub> O <sub>3</sub>	b.d.	b.d.	b.d.	0.01	0.03	b.d.	0.04	0.01	0.05	0.02	0.02	b.d.	0.02	b.d.	0.00
FeO	8.71	7.76	8.11	7.15	4.33	7.44	7.49	6.92	20.74	20.94	6.68	16.28	6.83	10.17	8.38
MnO	0.17	0.17	0.18	0.15	0.06	0.18	0.20	0.11	0.65	0.65	0.15	0.38	0.18	0.20	0.17
MgO	49.86	50.63	50.62	51.29	53.41	50.88	50.91	51.81	39.74	41.33	51.74	43.63	51.68	49.82	50.95
CaO	0.25	0.28	0.33	0.28	0.24	0.27	0.20	0.24	0.04	0.06	0.19	0.04	0.20	0.05	0.07
Cr <sub>2</sub> O <sub>3</sub>	b.d.	0.01	b.d.	0.01	0.46	b.d.	1.04	0.01	0.01	b.d.	b.d.	0.02	0.04	0.03	b.d.
NiO	0.18	0.15	0.14	0.20	0.16	0.17	0.16	0.22	0.02	0.07	0.25	0.10	0.24	0.32	0.21
Total	100.46	99.65	100.21	99.84	99.74	99.35	100.43	99.99	99.83	101.43	99.84	99.73	99.88	100.44	100.02
Fo (mol)	0.91	0.92	0.92	0.93	0.96	0.92	0.92	0.93	0.77	0.78	0.93	0.83	0.93	0.90	0.92

Sample	KT31G-23	KT31G-69	KT32-118	KT33-129	KT33-177	KT35-25	KT36-269	KT36-311	KT37-190	KT38-32	KT40-343	KT42-194	KT46-171	KT49-191	KT51-256
Lithology	Ch*	Ch	Du	Ch	Ch*	Hb	Ch*	Ch	Du	Du	Du	Du	Gb	Cp	Cp
SiO <sub>2</sub> (wt.%)	41.05	40.84	39.99	40.91	41.04	39.48	41.84	41.17	40.13	39.88	40.35	40.36	37.88	38.39	38.67
TiO <sub>2</sub>	b.d.	b.d.	0.02	0.01	0.01	b.d.	0.02	0.02	0.03	b.d.	0.02	0.03	b.d.	b.d.	b.d.
Al <sub>2</sub> O <sub>3</sub>	b.d.	b.d.	b.d.	b.d.	b.d.	b.d.	b.d.	b.d.	b.d.	b.d.	b.d.	b.d.	0.02	b.d.	b.d.
FeO	5.91	8.43	10.35	9.30	6.73	13.06	4.72	9.50	10.29	13.26	8.28	8.29	23.34	16.91	17.62
MnO	0.08	0.16	0.25	0.23	0.17	0.24	0.11	0.17	0.22	0.30	0.15	0.16	0.69	0.40	0.33
MgO	53.00	50.06	48.81	49.30	51.23	47.27	53.59	49.54	49.19	46.35	50.46	50.56	39.14	44.62	43.47
CaO	0.18	0.24	0.30	0.19	0.18	0.03	0.05	0.08	0.05	0.04	0.26	0.33	0.02	0.03	b.d.
Cr <sub>2</sub> O <sub>3</sub>	0.83	0.05	0.02	0.04	0.56	b.d.	0.85	0.03	0.03	0.02	0.05	0.01	b.d.	0.01	b.d.
NiO	0.15	0.18	0.16	0.15	0.15	0.15	0.16	0.11	0.14	0.13	0.18	0.17	0.03	0.12	0.12
Total	101.25	99.96	100.01	100.17	100.08	100.22	101.34	100.66	100.13	99.98	99.74	100.02	101.12	100.53	100.21
Fo (mol)	0.94	0.91	0.89	0.90	0.93	0.87	0.95	0.90	0.89	0.86	0.92	0.92	0.75	0.82	0.81

FeO = total iron content, NT = Nizhnii Tagil, KT = Kytlym, SB = Svetley Bor, Du = Dunite, Ch = Chromitite, Ch\* = inclusion in Spinel, Cp = Clinopyroxenite, Wh = Wehrlite, Gb = Gabbro, Hb = Hornblende, b.d. = below limit of detection.

Table 3  
Spinel compositions of selected samples from Uralian–Alaskan-type intrusions

Sample	NT2-167	NT5-106	NT12-148	SB18-49	SB20-28	SB30-231	KT31G-8	KT36-296	KT37-163	KT35-4b ex	KT35-4a ex	KT 35-4 orig.	KT35-1a ex	KT35-1b ex	KT35-1 core	KT 35-1 orig.	KT51-272	KT51-280
Lithology	Du	Ch	Du	Du	Cp	Hb	Ch	Ch	Du	Hb	Hb	Hb	Hb	Hb	Hb	Hb	Cp	Cp
TiO <sub>2</sub> (wt.%)	0.52	0.45	0.39	0.52	0.89	0.73	0.78	0.82	0.75	4.80	0.45	3.78	4.46	0.60	2.55	2.63	0.09	2.06
Al <sub>2</sub> O <sub>3</sub>	7.63	7.15	7.37	6.04	4.09	63.94	8.16	9.46	11.65	5.92	37.53	13.31	7.25	33.78	15.31	19.79	46.56	3.75
FeO <sub>m</sub>	34.41	30.12	30.83	50.10	70.09	16.10	36.51	40.63	46.44	67.62	30.11	58.86	60.80	30.94	53.00	46.69	26.11	76.40
MnO	0.51	0.36	0.51	0.62	0.59	0.45	0.34	0.39	0.56	0.47	0.31	0.43	0.53	0.33	0.42	0.43	0.21	0.29
MgO	8.22	11.83	7.75	4.39	0.37	10.33	9.90	6.74	5.64	3.31	11.33	5.19	3.56	10.74	5.33	6.95	11.25	1.12
Cr <sub>2</sub> O <sub>3</sub>	46.40	48.90	51.52	35.58	17.71	0.10	42.61	38.53	33.06	16.52	18.90	17.08	19.76	23.19	20.76	21.38	14.32	9.62
NiO	0.06	0.07	0.10	0.15	0.11	0.05	0.14	0.14	0.13	0.25	0.17	0.23	0.24	0.11	0.19	0.18	0.12	0.16
V <sub>2</sub> O <sub>3</sub>	0.06	b.d.	b.d.	0.04	0.20	b.d.	0.08	0.10	0.12	0.46	0.16	0.39	0.32	0.13	0.26	0.23	0.03	0.26
ZnO	0.18	b.d.	0.21	0.27	0.12	3.66	b.d.	0.14	0.23	0.06	0.43	0.15	0.10	0.48	0.18	0.28	1.36	0.11
CoO	0.09	b.d.	0.10	0.12	0.03	0.19	0.05	0.03	0.11	0.13	0.11	0.12	0.12	0.12	0.13	0.12	0.12	0.04
Total	98.03	98.87	98.80	97.83	94.19	95.54	98.59	97.11	98.70	99.56	99.56	99.56	97.18	100.42	98.14	99.11	100.18	93.82
Cr/(Cr+Al)	0.80	0.82	0.82	0.80	0.74	<0.01	0.78	0.73	0.66	0.65	0.25	0.46	0.65	0.32	0.48	0.42	0.17	0.63
Fe <sup>3+</sup> /(Cr+Al+Fe <sup>3+</sup> )	0.21	0.21	0.15	0.37	0.63	<0.01	0.26	0.24	0.31	0.60	0.12	0.46	0.51	0.13	0.38	0.30	0.06	0.76
Fe <sup>2+</sup> /(Mg+Fe <sup>2+</sup> )	0.58	0.42	0.60	0.76	0.98	0.47	0.51	0.49	0.71	0.85	0.50	0.76	0.83	0.52	0.75	0.68	0.51	0.94
FeO <sub>calc</sub>	20.04	15.00	20.81	25.90	31.12	16.10	18.61	18.17	25.34	32.26	20.29	29.47	30.73	21.00	27.85	26.13	20.77	31.24
Fe <sub>2</sub> O <sub>3calc</sub>	15.96	16.80	11.43	27.90	43.31	<0.01	20.48	19.40	24.12	39.30	10.91	32.67	33.41	11.05	27.95	22.84	5.93	50.18

FeO<sub>m</sub> = measured iron content, FeO<sub>calc</sub> and Fe<sub>2</sub>O<sub>3calc</sub> calculated from stichiometry, NT = Nizhni Tagil, KT = Kytlym, SB = Svetley Bor, Du = Dunite, Ch = Chromitite, Cp = Clinopyroxenite, Gb = Gabbro, Hb = Hornblendite, ex = exsolved spinel, orig. = composition before exsolution calculated from area analysis, b.d. = below limit of detection.

Table 4  
Clinopyroxene compositions of selected samples from Uralian–Alaskan-type intrusions

Sample	NT1-69	NT1T6-14	NT12-114	NT13-115	SB16-64	SB22-88	SB30-246	KT31F-249	KT33-132	KT37-148	KT38-69	KT49-110	KT51-245	KT51-247	KT51-251
Lithology	Du	Vn	Du	Cp	Vn	Cp	Hb	Ch	Ch	Du	Wh	Cp	Cp	Cp	Cp
Position	M	M	M	M	M	M	M	M	M	M	M	M	C	R	M
SiO <sub>2</sub> (wt.%)	54.03	54.58	54.06	52.22	53.40	50.88	43.23	53.08	54.38	54.64	53.93	51.63	52.83	51.72	51.45
TiO <sub>2</sub>	0.10	0.09	0.09	0.32	0.18	0.33	1.63	0.11	0.05	0.09	0.23	0.28	0.12	0.23	0.29
Cr <sub>2</sub> O <sub>3</sub>	0.33	0.81	0.39	0.03	0.53	0.07	b.d.	0.17	0.35	0.14	0.45	0.14	0.48	0.52	0.39
Al <sub>2</sub> O <sub>3</sub>	0.80	0.93	0.72	2.57	1.46	3.43	10.73	0.52	0.81	0.41	1.57	2.33	1.26	1.95	2.65
FeO*	2.26	1.84	1.39	5.62	2.37	5.46	9.93	1.39	1.85	1.49	3.42	4.54	4.27	4.86	5.08
MnO	0.04	0.04	0.05	0.14	0.07	0.10	0.19	0.02	0.02	0.05	0.11	0.13	0.09	0.13	0.19
MgO	17.60	16.93	17.42	15.17	17.14	15.34	9.48	17.56	16.85	17.30	16.39	16.14	17.41	16.46	16.00
CaO	25.29	24.28	25.31	23.48	24.60	23.31	23.70	25.32	25.25	25.37	23.58	23.89	22.36	22.71	22.35
Na <sub>2</sub> O	0.24	0.47	0.36	0.33	0.30	0.27	0.37	0.07	0.21	0.07	0.29	0.16	0.20	0.22	0.25
Total	100.70	100.04	99.82	99.93	100.08	99.20	99.30	98.27	99.83	99.59	100.03	99.25	99.06	98.86	98.69
Mg/(Fe+Mg)	0.93	0.94	0.96	0.83	0.93	0.83	0.63	0.96	0.94	0.95	0.90	0.86	0.88	0.86	0.85
Ba (ppm)	1.8	4.6	b.d.	0.1	0.2	0.1	n.m.	1.8	1.3	2.0	1.5	1.5	b.d.	b.d.	b.d.
Th	0.003	0.046	0.003	0.014	0.020	0.008	n.m.	0.002	0.017	0.026	0.007	0.018	0.007	0.011	0.018
U	0.005	0.018	b.d.	0.002	0.012	0.004	n.m.	b.d.	0.007	0.004	0.004	0.007	0.002	0.003	0.004
La	0.07	1.45	0.17	1.58	1.04	0.40	n.m.	0.06	1.07	0.42	0.46	0.77	0.41	0.60	0.80
Ce	0.19	3.72	0.42	5.05	3.34	1.67	n.m.	0.22	2.85	1.53	1.81	2.78	1.33	2.14	2.88
Sr	24	191	26	214	140	57	n.m.	8	102	40	65	79	43	47	48
Pr	0.03	0.61	0.07	0.97	0.75	0.43	n.m.	0.04	0.44	0.35	0.40	0.62	0.24	0.41	0.56
Nd	0.2	3.1	0.4	5.3	4.1	2.8	n.m.	0.2	2.1	1.9	2.5	3.7	1.4	2.4	3.4
Hf	0.10	0.15	0.10	0.45	0.16	0.30	n.m.	0.07	0.12	0.90	0.21	0.25	0.05	0.10	0.28
Sm	0.14	0.90	0.29	1.76	1.24	1.08	n.m.	0.08	0.58	0.72	0.85	1.22	0.42	0.77	1.15
Zr	1.7	3.4	1.5	9.3	2.8	5.2	n.m.	0.9	3.2	13.6	3.6	5.0	1.2	2.8	5.9
Eu	0.07	0.32	0.17	0.56	0.41	0.37	n.m.	0.03	0.19	0.22	0.29	0.41	0.16	0.27	0.38
Gd	0.37	0.97	0.66	1.88	1.20	1.24	n.m.	0.15	0.69	0.92	0.88	1.32	0.52	0.90	1.33
Tb	0.09	0.13	0.13	0.25	0.14	0.20	n.m.	0.03	0.10	0.20	0.13	0.19	0.07	0.13	0.21
Dy	0.54	0.71	0.66	1.37	0.73	1.18	n.m.	0.21	0.55	1.38	0.80	1.04	0.43	0.78	1.26
Ho	0.08	0.12	0.12	0.25	0.14	0.23	n.m.	0.04	0.09	0.26	0.16	0.19	0.09	0.17	0.25
Er	0.20	0.26	0.28	0.63	0.33	0.60	n.m.	0.09	0.19	0.83	0.41	0.50	0.22	0.43	0.67
Tm	0.02	0.03	0.03	0.09	0.04	0.08	n.m.	0.01	0.02	0.08	0.06	0.06	0.03	0.06	0.08
Yb	0.16	0.20	0.16	0.48	0.25	0.48	n.m.	0.07	0.14	0.58	0.43	0.42	0.21	0.37	0.57
Lu	0.02	0.03	0.03	0.08	0.04	0.06	n.m.	0.01	0.02	0.07	0.07	0.05	0.03	0.06	0.09

FeO\* = all iron measured as FeO. NT = Nizhnii Tagil, KT = Kytlym, SB = Svetley Bor, Du = Dunite, Vn = Diopside vein in dunite, Wh = Wehrlite, Ch = Chromitite, Cp = Clinopyroxenite, Hb = Hornblende, M = matrix, C = core of phenocryst, R = rim of phenocryst, b.d. = below limit of detection, n.m. = not measured.

the gabbros to 3.6–12.6 in the clinopyroxenites and is therefore significantly higher than that observed in most mantle melts and upper mantle peridotites.

### 3.2. Mineral chemistry

#### 3.2.1. Chemical composition of olivine

Olivine is present in all rock types and Table 2 summarizes its chemical composition in selected samples. In dunites, olivine shows a rather large compositional variation as the Forsterite (Fo) content ranges from 86 to 94 (Fig. 3). It is important to note that the forsterite content of olivine in the vicinity of the chromitite is high (Fo<sub>90–93</sub>), but the highest Fo contents (Fo<sub>93–96</sub>) are observed in olivine inclusions in spinel from the chromitites (Fig. 3). Olivine in the other rock types has lower Fo values decreasing systematically from Fo<sub>84–86</sub> in the hornblendites, Fo<sub>80–83</sub> in the clinopyroxenites to Fo<sub>74–84</sub> in the gabbros.

Nickel in olivine shows a systematic positive correlation with the Fo content (Fig. 3). This variation follows the lower limit of a global field defined by olivine which crystallized from different mantle-derived

magma types. However, Fo-rich olivine (Fo<sub><89</sub>), especially inclusions of olivine in chromitite, have relatively low and rather constant Ni concentrations and many are outside of this field (Fig. 3).

#### 3.2.2. Chemical composition of spinel

Spinel is present as an accessory phase in all rock types and as the main component in the chromitites. This mineral displays a wide compositional range with regard to its major components, Mg, Fe<sup>2+</sup>, Cr, Fe<sup>3+</sup>, Al and Ti (Table 3; Figs. 4 and 5).

The accessory spinel in the dunites follows characteristic trends, which in most cases can even be observed in one single thin section (Figs. 4a and 5a). These trends divide the spinel population into three different groups. In Fig. 4a the trend starts at a composition of Al<sub>13</sub>Cr<sub>63</sub>Fe<sup>3+</sup><sub>24</sub> and evolves in group I due to the exchange of Cr and Fe<sup>3+</sup> towards Al<sub>13</sub>Cr<sub>50</sub>Fe<sup>3+</sup><sub>37</sub>. At this point Al is replaced with Fe<sup>3+</sup> towards a composition of Al<sub>0</sub>Cr<sub>51</sub>Fe<sup>3+</sup><sub>49</sub> (group II spinel Fig. 4a). Subsequently Cr is substituted in group III with Fe<sup>3+</sup> until the spinel composition reaches the miscibility gap (Al<sub>0</sub>Cr<sub>35</sub>Fe<sup>3+</sup><sub>65</sub>) or forms pure magnetite, which can be sometimes observed

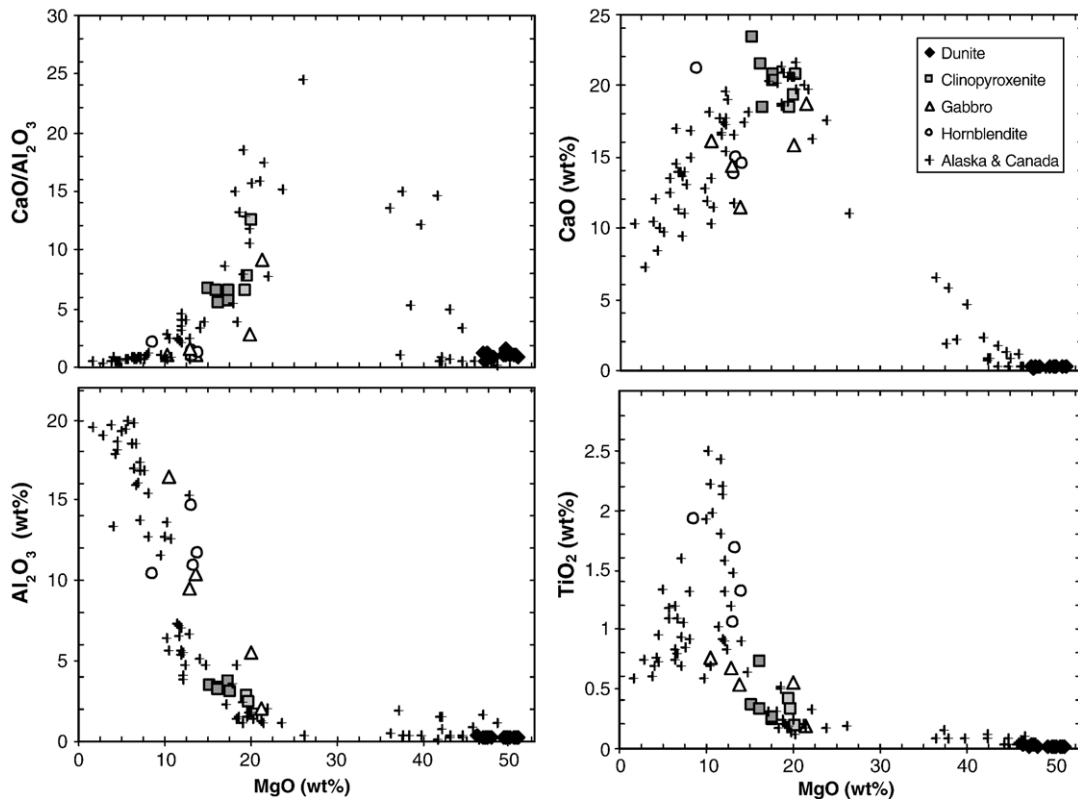


Fig. 2. Correlation diagrams for major oxides of rocks from Uralian–Alaskan-type complexes in the UPB. Comparison with other occurrences in the Cordillera of Alaska and W-Canada (Wyllie, 1967; Findlay, 1969; Himmelberg and Loney, 1995).

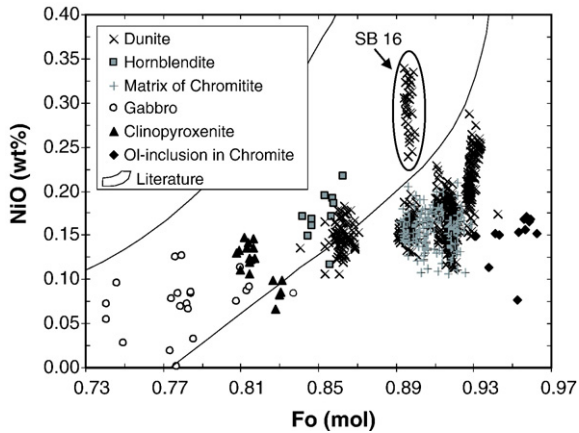


Fig. 3. Chemical composition of olivine in different lithologies from the Uralian–Alaskan-type complexes in the Tagil Magnitogorsk zone of the Ural mountains. Fo-rich samples (except sample SB16) have low Ni contents if compared with the global trend. Literature data are from the GEOROC-database (<http://georoc.mpch-mainz.gwdg.de/georoc/>).

as rims around chromite grains (Fig. 4a–c). The  $\text{TiO}_2$  content (not shown) rises from 0.4 to 0.8 wt.% in groups I and II spinel until Al is substituted with Cr and  $\text{Fe}^{3+}$ , when it decreases to 0.05 wt.% in group III spinel. Similarly  $\text{Fe}^{2+}/(\text{Mg} + \text{Fe}^{2+})$  and  $\text{Fe}^{3+}/(\text{Cr} + \text{Al} + \text{Fe}^{3+})$  increase from 0.55 to 0.85 and 0.15 to 0.55, respectively in groups I and II (Fig. 5a). In Al-free spinel (group III)  $\text{Fe}^{2+}/(\text{Mg} + \text{Fe}^{2+})$  remains fairly constant close to 0.9, but  $\text{Fe}^{3+}/(\text{Cr} + \text{Al} + \text{Fe}^{3+})$  increases to 1 (Fig. 5a, d). The Cr/(Cr + Al) is constant around 0.8 in group I. However, the replacement of Al with  $\text{Fe}^{3+}$  in group II causes an increase in Cr/(Cr + Al) to about 1.

There is also a systematic chemical difference between spinel from different complexes. For example, accessory spinel from Nizhnii Tagil tends to have lower  $\text{TiO}_2$  and  $\text{Al}_2\text{O}_3$ -concentrations and higher Cr/(Cr + Al) values than those of Kytlym and Svetley Bor (Figs. 4 and 5e–f, Table 3).

The chemical composition of spinel in the chromitites is considerably less variable than that of accessory spinel in the dunites. We only observe Cr-rich spinel (Fig. 4c) and their chemical variations are similar to those observed for accessory spinel belonging to group I. In Kytlym some of the spinels have magnetite-rich compositions. Like the accessory spinel in the dunites, the chromitite spinel from Nizhnii Tagil has higher Cr/(Cr + Al) values and lower  $\text{TiO}_2$  contents than that from

Kytlym (Figs. 4c and 5f, Table 3). The cataclastic deformation of spinel observed in some chromitites has no influence on their chemical composition.

Spinel from clinopyroxenites, hornblendites and gabbros generally has low  $\text{Cr}_2\text{O}_3$  contents, up to 18 wt.% in clinopyroxenites and less than 4 wt.% in hornblendites and gabbros (Table 3). Thus, most of the spinel has a magnetite-rich composition (Fig. 4d). In hornblendites (SB30, SB29b) some spinels are hercynites and have elevated ZnO contents (up to 3.6 wt.%).

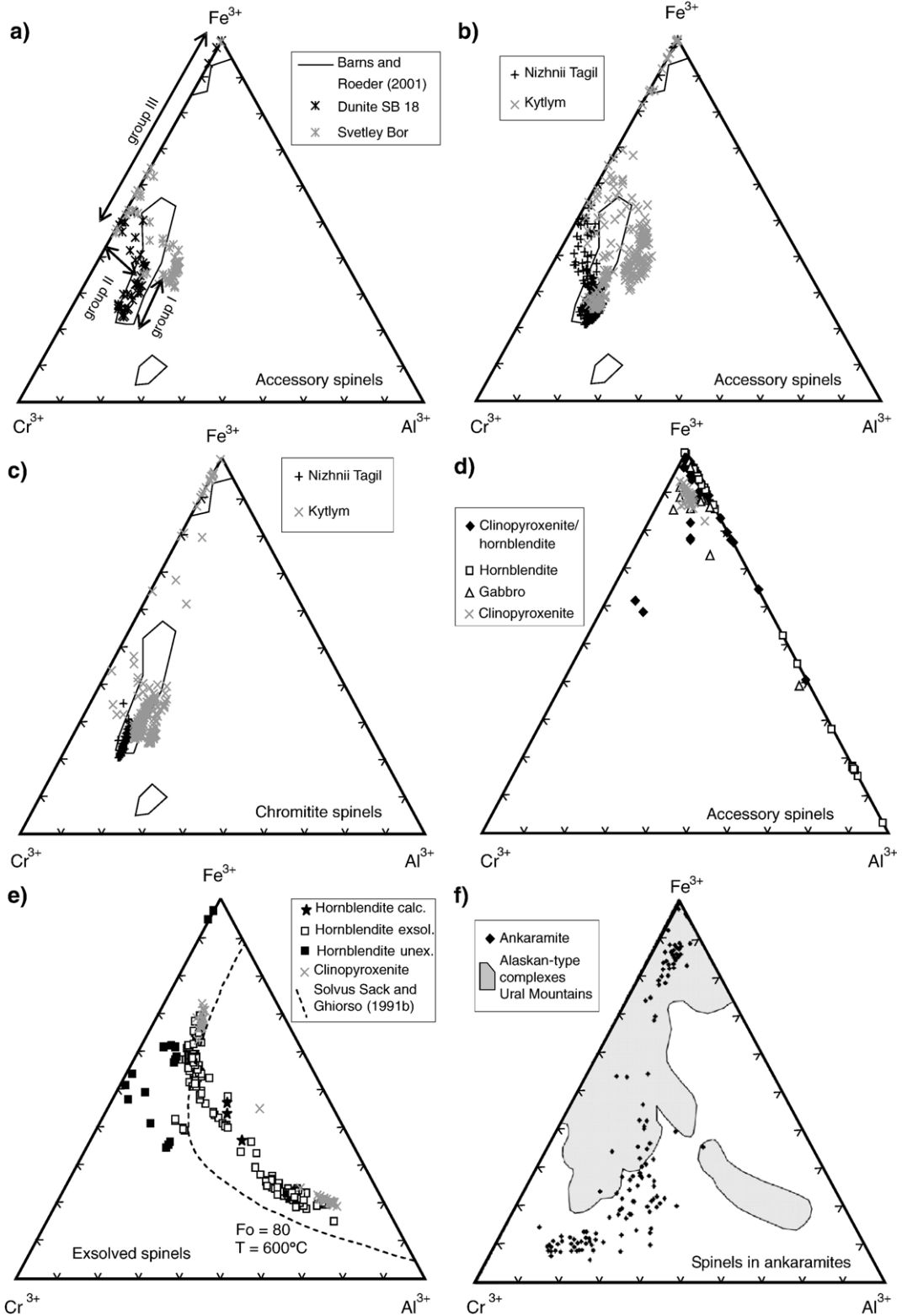
### 3.2.3. Major and trace element concentrations in clinopyroxene

Clinopyroxene is present in all rock types. In dunites it mainly appears as a xenomorphic interstitial phase. It occurs as an idiomorphic to hypidiomorphic cumulate phase in clinopyroxenites, hornblendites and gabbros, where exsolutions of titanomagnetite often form a visible zonation. Clinopyroxene is also present in the chromitites as interstitial phase and as inclusions in spinel. Its composition is similar to that of interstitial grains occurring in the dunites. In Svetley Bor and Nizhnii Tagil veins of green, idiomorphic clinopyroxene crosscut some of the dunites. Almost all clinopyroxenes are diopsides, but some augite is found in the clinopyroxenites and the dunite (Fig. 6 Table 4).

The clinopyroxene shows chemical variations which are controlled by the host lithology. For example, a negative correlation between  $\text{Al}_2\text{O}_3$  and  $\text{Mg}/(\text{Mg} + \text{Fe})$  is displayed in Fig. 7a where clinopyroxene from dunites has the lowest contents of  $\text{Al}_2\text{O}_3$ , MnO and  $\text{TiO}_2$  but they systematically increase towards clinopyroxenite, gabbro and hornblende, while  $\text{SiO}_2$  contents systematically decrease (not shown). Clinopyroxene in one hornblende from Svetley Bor (SB30) has  $\text{Al}_2\text{O}_3$  contents up to 12.3 wt.%. This requires an extensive incorporation of the Tschermak component and explains the high proportion of the wollastonite component (>50; Fig. 6).

A positive correlation of the middle and heavy REE contents with  $\text{Al}_2\text{O}_3$ , FeO, and  $\text{TiO}_2$  and a negative one with  $\text{Mg}/(\text{Mg} + \text{Fe})$  can be observed for all lithologies. The distribution of the middle and heavy REE is similar to that of  $\text{Al}_2\text{O}_3$  in that, for example, Lu concentrations increase from dunite to clinopyroxenite (Fig. 7b). For Nb, U, Th and Sr no clear correlation with the major elements and the REEs is seen.

Fig. 4. Distribution of trivalent cations in spinel from Uralian–Alaskan-type complexes and ankaramites. These include: a) accessory spinel Svetley Bor, b) accessory spinel Kytlym and Nizhnii Tagil, c) spinel from chromitite, d) accessory spinel from clinopyroxenite, hornblende and gabbro, e) exsolved spinel calc. = calculated spinel composition before exsolution, and f) comparison with spinel from ankaramites (Barsdell and Smith, 1989; Barsdell, 1989; Nono et al., 1994; Mossman et al., 2000). Compositional fields for Uralian–Alaskan-type complexes are from Barnes and Roeder (2001). The solvus curve for spinel in e) was calculated for 600 °C and  $\text{Fo}_{90}$  olivine by Sack and Ghiorso (1991b).



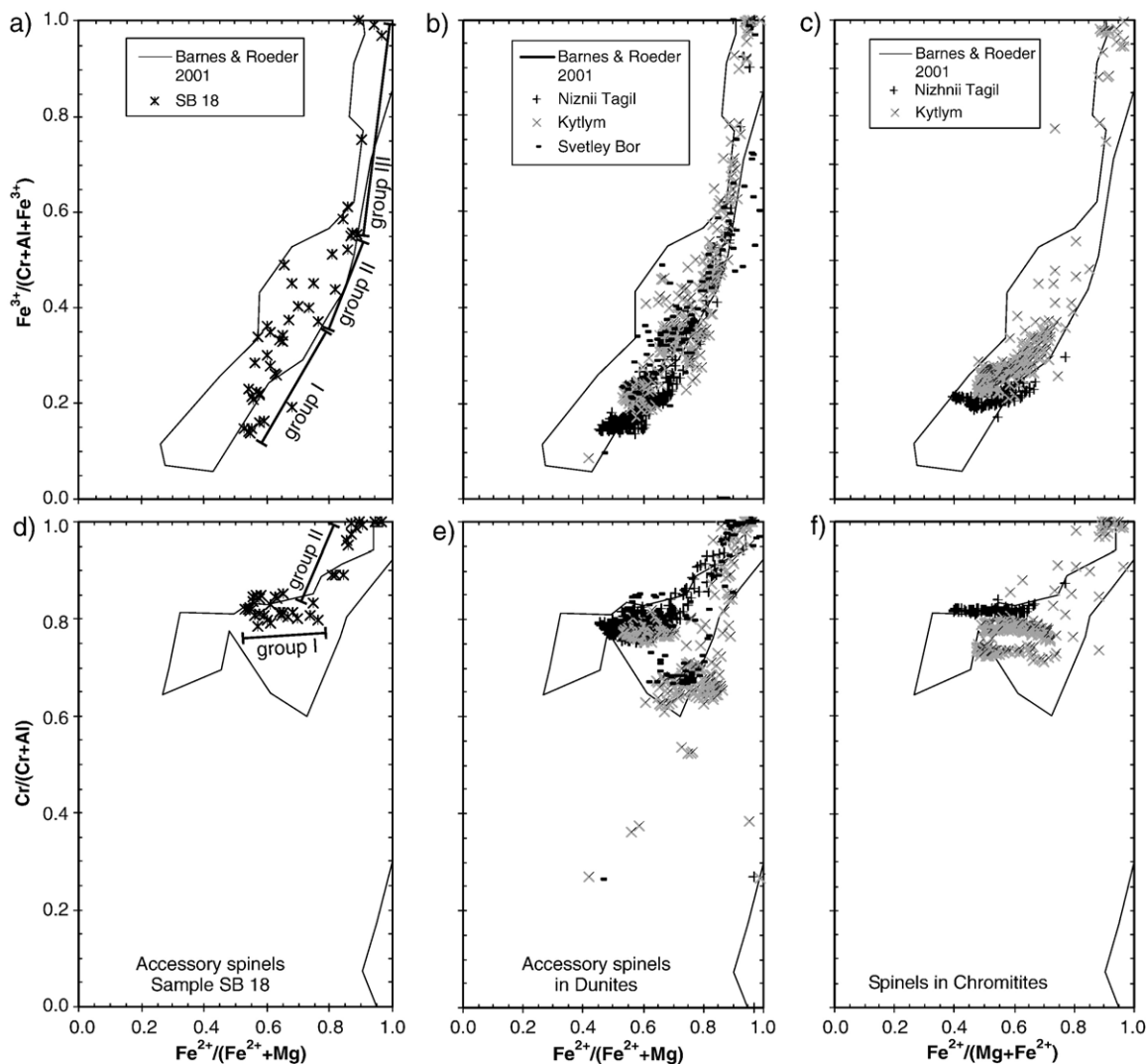


Fig. 5. Variation of  $Fe^{2+}/(Fe^{2+}+Mg)$ ,  $Fe^{3+}/(Cr+Al+Fe^{3+})$  and  $Cr/(Cr+Al)$  in spinel from Uralian–Alaskan-type intrusions. (a, d) accessory spinel in sample SB18, (b, e) accessory spinel in dunite, (c, f) spinel in chromitite.

The REE patterns (primitive mantle normalized) for all diopside, irrespective of rock type and sample location, have a convex shape with a maximum enrichment of MREE (Fig. 8). However, the concentrations of different grains within a single sample could vary by a factor of 2–6, and the total spread is about one and a half orders of magnitude. All samples show a linear correlation among the middle and heavy REE (Fig. 9a). However, correlations with highly incompatible elements (La) are poor, as demonstrated by variable La/Lu ratios in Fig. 9b.

Many extended mantle normalized trace element patterns of clinopyroxene run virtually parallel, regardless of the rock type. The lowest trace element concentrations are measured on interstitial grains in dunites, diopside

veins crosscutting dunite and in chromitites. The concentrations increase systematically in the clinopyroxenes (Fig. 8). Most of the clinopyroxene grains show positive anomalies for Sr and negative anomalies for Th, U, Nb, Ta, Hf, Zr and Ti (Fig. 8).

#### 4. Discussion

Major element composition and mineralogical observations reveal a successive crystallisation of olivine + chromite forming dunite, olivine + chromite + clinopyroxene forming wehrlite, clinopyroxene + chromian magnetite forming clinopyroxenite and clinopyroxene + spinel + plagioclase + phlogopite  $\pm$  k-feldspar  $\pm$  nepheline forming gabbro. The major element composition and

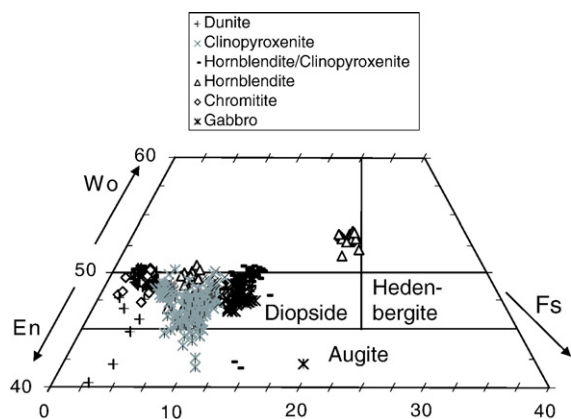


Fig. 6. Classification of clinopyroxene from Uralian–Alaskan-type complexes.

trends in whole rock samples closely follow published data from British Columbia and Canada (Fig. 2) (Wyllie, 1967; Findlay, 1969; Himmelberg and Loney, 1995). The high  $\text{CaO}/\text{Al}_2\text{O}_3$  ratios in all rock types and their alkaline affinity are well established features for all Uralian–Alaskan-type complexes.

Himmelberg and Loney (1995) observed well defined negative correlations between decreasing  $\text{MgO}$  and the increase of incompatible elements, such as  $\text{Al}_2\text{O}_3$ , in both whole rocks and minerals. Therefore, these authors suggested that  $\text{MgO}$  and  $\text{Al}_2\text{O}_3$  represent good tracers of fractionation processes in the parental magmas of Uralian–Alaskan-type complexes in Alaska. However, this study observes remarkably large variations in the spinel composition and the concentrations of incompatible trace elements in clinopyroxene even on the scale of a single thin section. These characteristics cannot simply be primary features. The concentration of an element in minerals as well as the mineral composition in cumulate rocks can potentially be changed by several late processes including modification due to interaction with late interstitial or percolating melts and fluids and subsolidus equilibration with neighbouring grains.

#### 4.1. Subsidius equilibration of spinel

The chemical composition of spinel from the Uralian complexes is similar to those from Uralian–Alaskan-type complexes world wide (Figs. 4 and 5; Barnes and Roeder, 2001). These complexes are characterized by a complex and multifaceted spinel chemistry.

In a clinopyroxenite (KT 51) from Tilay mountain (Kytlym) and an olivine- and clinopyroxene-rich hornblende dyke (KT35) intruding the dunite from Kosiva mountain (Kytlym) exsolved spinel can be found (Fig. 4e),

which coexist with olivine ( $\text{Fo}_{80}$ ). Spinel in the clinopyroxenite from Tilay mountain (Kytlym) exsolved a picotitic phase at  $\text{Al}_{65}\text{Cr}_{14}\text{Fe}_{21}^{3+}$  and a chromian titanomagnetite at  $\text{Al}_{12}\text{Cr}_{21}\text{Fe}_{67}^{3+}$  with 2.5 wt.%  $\text{TiO}_2$  (Fig. 4e, Table 3). Fig. 10 shows the element maps of two exsolved spinel grains from sample KT35. In the first grain the Al-rich and Fe–Ti-poor spinel phases occur as blebs in a matrix of Al-poor and Fe-rich spinel (Fig. 10a). Both phases do not indicate any zonation. The centre of the other grain from the same sample is zoned and separated by sharp boundaries from the rim of the grain which predominantly consists of an Al- and Mg-rich chromian spinel with low Fe and Ti concentrations (Fig. 10a). This spinel exsolved into a chromian picotite  $\text{Al}_{57}\text{Cr}_{23}\text{Fe}_{20}^{3+}$  and a chromian titanomagnetite  $\text{Al}_{12}\text{Cr}_{30}\text{Fe}_{58}^{3+}$  with 3–7 wt.%  $\text{TiO}_2$ . The centre of this grain is zoned, because the Cr content decreases from the core towards the phase boundary. The Cr content is a little higher in the Al-rich spinel (Fig. 10b). On the basis of an area analysis of the element maps, the initial spinel composition is  $\text{Al}_{29}\text{Cr}_{25}\text{Fe}_{46}^{3+}$  for the first

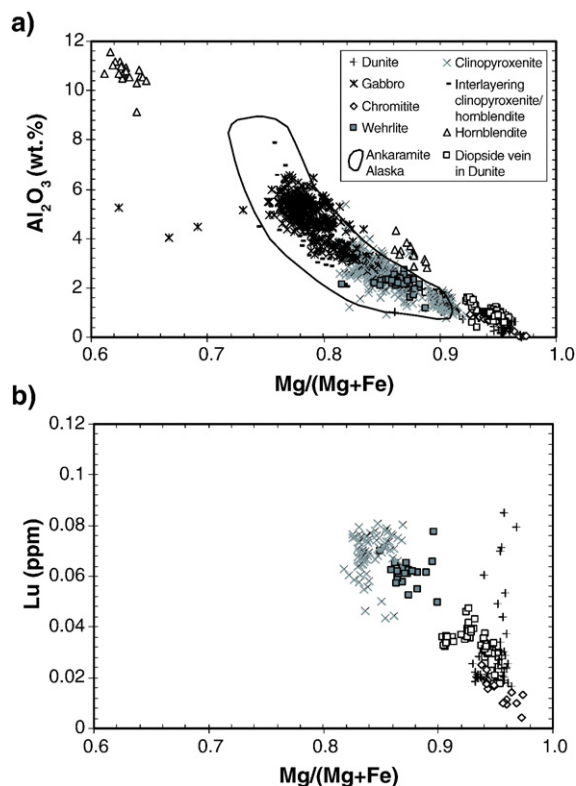


Fig. 7. a)  $\text{Al}_2\text{O}_3$  content and the  $\text{Mg}/(\text{Mg}+\text{Fe})$  in clinopyroxene from Uralian–Alaskan-type intrusions. Data for Ankarinites are from Irvine (1973). The systematic decrease of  $\text{Mg}\#$  and the decrease of  $\text{Al}_2\text{O}_3$  monitors the evolution of the parental melt. b) Lu content decreases with increasing  $\text{Mg}/(\text{Mg}+\text{Fe})$  in clinopyroxene.

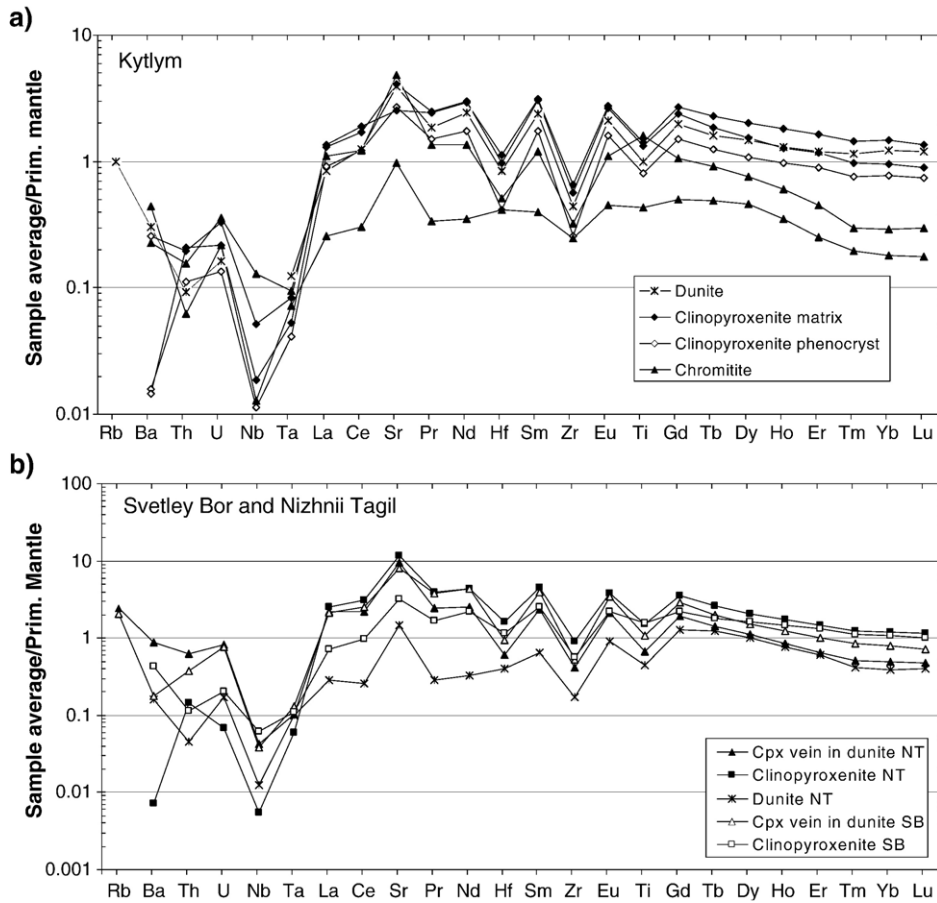


Fig. 8. Average trace element concentrations in diopside for a) Kytlym, b) Svetley Bor (SB) and Nizhnii Tagil (NT). Primitive mantle data are from Hofmann (1988).

grain and  $\text{Al}_{35}\text{Cr}_{28}\text{Fe}^{3+}_{37}$  for the second grain (Table 3). These compositions are very similar but they are enriched in  $\text{Al}_2\text{O}_3$  and  $\text{TiO}_2$  (2.4–4.8 wt.%) compared to unexsolved spinel in the same sample (Fig. 4e). Similar spinel exsolutions have been observed in the Uktus massif, another Uralian–Alaskan-type complex in the Ural (Garuti et al., 2003), and in the Iwanai-dake peridotite complex in Japan (Tamura and Arai, 2005).

However, the compositions of the exsolved spinels do not follow the solvus calculated for chromite coexisting at 600 °C with an olivine of  $\text{Fo}_{80}$ , because most of them are too Al-rich (Fig. 4e; Sack and Ghiorso, 1991b). Estimates of solvus curves at higher or lower temperatures do not improve the fit. Chashchukhin et al. (2002) demonstrated that the Ti content of spinel strongly influences the temperature estimates and that the commonly used olivine–spinel thermometers underestimate equilibrium temperatures. Thus, the high content of  $\text{TiO}_2$  in this spinel potentially explains the difference

between the observed and calculated spinel compositions in Fig. 4e.

The variation seen in group III spinel from dunites can be entirely ascribed to subsolidus reactions (Fig. 4a, b, c). It is partly the result of the expansion of the solvus of ternary spinel towards Cr–Fe<sup>3+</sup>-rich compositions with decreasing temperature. In addition, some of the Fe-rich spinel (magnetite) probably is an alteration product formed during the serpentinization of the rocks (Figs. 4 and 5).

Group II spinel displays a rather unusual evolution from Cr–Al-rich to Al-poor spinel (Fig. 4a,b). In addition, the Al-depletion is accompanied by a coherent increase of Fe<sup>2+</sup> and Fe<sup>3+</sup> (Fig. 5). This cannot represent a primary crystallization trend, because this process should produce a decrease in Cr, but not affect  $\text{Al}_2\text{O}_3$  to any significant degree. Expansion of the ternary spinel solvus towards Fe–Cr-spinel at temperatures below 600 °C is also an unlikely explanation. This exsolution would produce a spinel with similar  $\text{Al}_2\text{O}_3$  contents and not decreasing

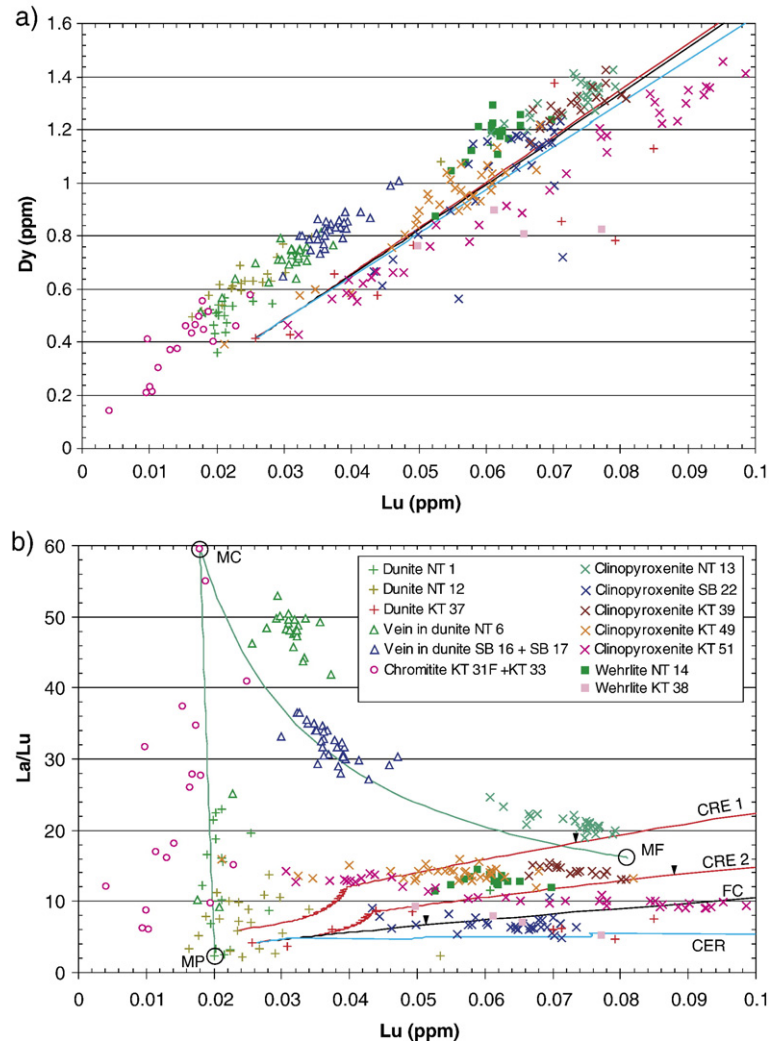


Fig. 9. REE variation in clinopyroxene from dunites, clinopyroxenites and chromitites from Uralian–Alaskan-type complexes in the Urals. These include a) diagram of Lu vs. Dy. b) diagram of Lu vs. La/Lu. Models calculated for two types of periodically tapped and replenished magma chambers are shown. CER model (blue dotted line): 5 cycles of 40% crystallization, 30% tapping, 30% recharge. CRE model (red dashed lines): 10 cycles of 40% crystallization, 10% recharged, 10% erupted. The last cycle is followed by fractional crystallization of the residual melt. Tick marks indicate the clinopyroxene composition after 70% fractional crystallization. MC, MF, MP represent end members of mixing lines (green solid lines) which explain the chemical variation in clinopyroxene from chromitite and diopside veins in dunites. For details see text.

$\text{Al}_2\text{O}_3$  contents as observed here (Sack and Ghiorso, 1991a,b). Equilibration with surrounding diopside under subsolidus conditions may influence the composition of chromian spinel. If this is the case, clinopyroxene could gather the  $\text{Al}_2\text{O}_3$  from the spinel leaving behind Al-poor chromites.

#### 4.2. Olivine and chromian spinel as monitors of the evolution of the parental magma

The compositional variation observed in group I spinel from dunites, where  $\text{Fe}^{2+}/(\text{Mg} + \text{Fe}^{2+})$  and  $\text{Fe}^{3+}$  coherently

increase while  $\text{Cr}/(\text{Cr} + \text{Al})$  decreases (Figs. 4 and 5), is consistent with the crystallization of Fo-rich olivine and chromian spinel from a MgO-rich melt (Roeder, 1994). Interestingly, spinel from different complexes follows different trends due to variable  $\text{Cr}/(\text{Cr} + \text{Al})$ . For example accessory spinel and spinel from chromitites from Kytlym have systematically higher  $\text{Cr}/(\text{Cr} + \text{Al})$  than those from Nizhnii Tagil (Fig. 5e, f). The diverse  $\text{Cr}/(\text{Cr} + \text{Al})$  are due to variable  $\text{Al}_2\text{O}_3$  content in the spinel, and this is probably a fingerprint of the  $\text{Al}_2\text{O}_3$  content of the parental melt.

Olivine also shows a substantial compositional variation as the Fo-content ranges from 74 to 96 mol%

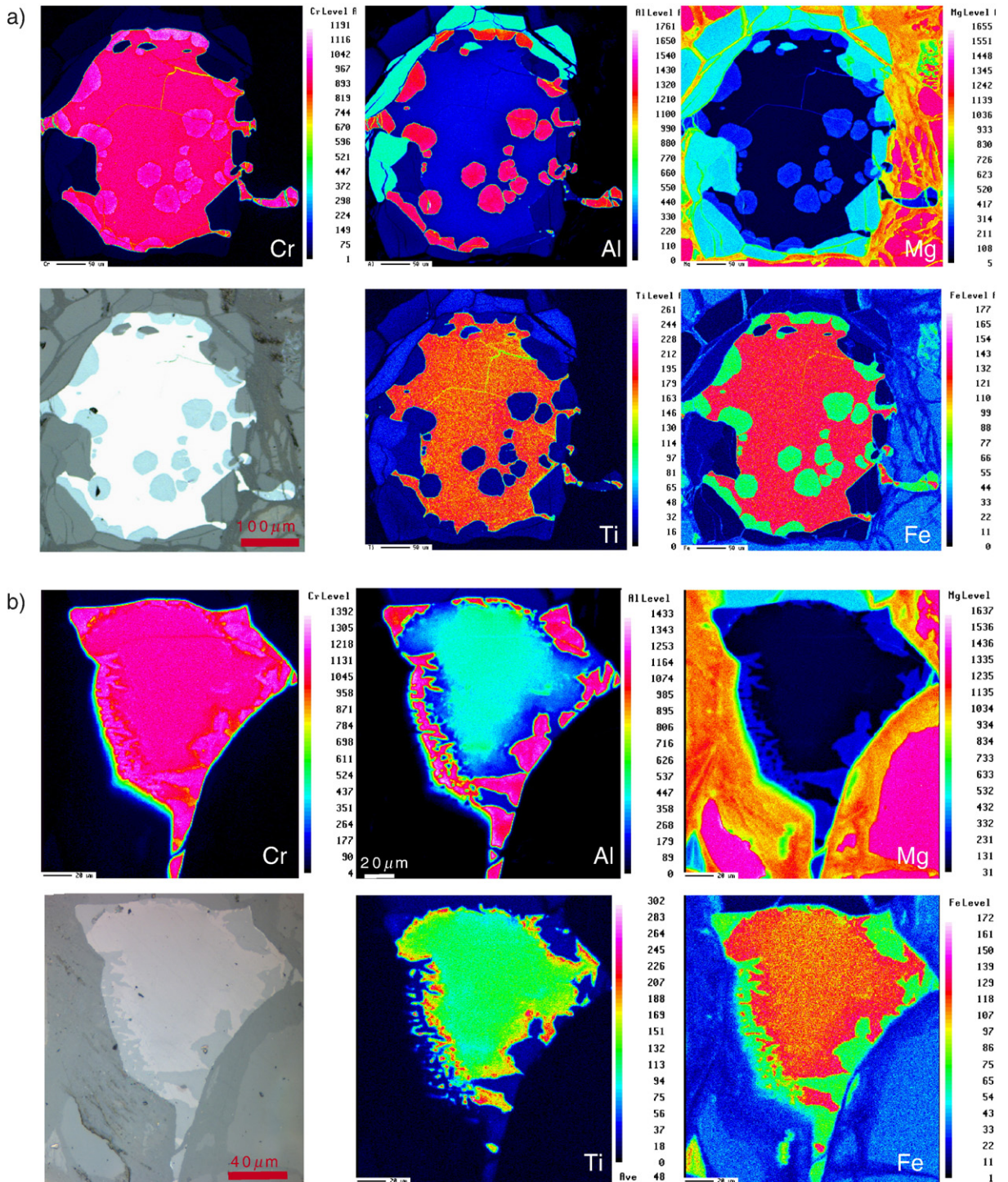


Fig. 10. Element maps for Al, Fe, Mg, Ti, and Cr and the reflected light image of two exsolved spinel grains from an ol–cpx–hornblende dike crosscutting a dunite (Kytlym complex). (a) shows an entirely equilibrated spinel grain. (b) shows a spinel grain with a zoned core.

(Fig. 3, Table 2). The highest Fo-content ( $>Fo_{93}$ ) occurs in olivine inclusions in chromite (Fig. 3) together with unusually high  $Cr_2O_3$  contents of up to 0.85 wt.%. In

dunite–chromite cumulates from layered intrusions and ophiolite complexes and particularly in inclusions of olivine in chromite, the Fo-content increases with

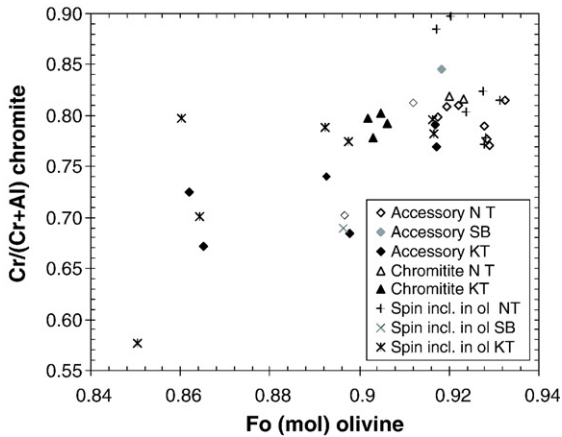


Fig. 11. The mean Fo component in olivine and Cr/(Cr+Al) in spinel monitor the early evolution of the parental magma from the Uralian–Alaskan-type complexes. SB = Svetley Bor, NT = Nizhnii Tagil, KT = Kytlym.

increasing proportions of chromite due to subsolidus exchange of Fe–Mg (e.g. Jackson, 1969; Lehmann, 1983; Melcher et al., 1997). A vacancy coupled subsolidus substitution of  $\text{Cr}^{3+}$  between spinel and olivine could explain the high Cr concentration for olivine inclusions in chromite (Lehmann, 1983). At lower Fo contents ( $\text{Fo} < 93$ ), however, the combined decrease in Ni and Fo content in olivine from dunite, clinopyroxenite and gabbro monitors the crystallization of the parental melts.

Fig. 11 shows the variation of the average forsterite content in olivine and the average Cr/(Cr+Al) for group I spinel in each sample. These samples define a positive correlation as expected during the joint fractional crystallization of olivine and chromite (Roeder, 1994). This variation is narrow in Nizhnii Tagil and restricted to the primitive part of the trend with high Cr/(Cr+Al) in spinel and high Fo contents in olivine ( $\text{Cr}/(\text{Cr}+\text{Al}) > 0.76$ ,  $> \text{Fo}_{91}$ ). Dunites from Kytlym show a much larger variation, but the most primitive samples overlap with those from Nizhnii Tagil. The greater heterogeneity at Kytlym reflects the larger extent of fractional crystallization of the parental magma. The crystallization of spinel with high Cr/(Cr+Al) ( $\sim 0.80$ ) and low  $\text{Al}_2\text{O}_3$  contents and MgO-rich olivine ( $\text{Fo}_{92-93}$ ) indicates that the parental magma of the Uralian–Alaskan-type complexes was of ultramafic composition with a high MgO ( $> 15$  wt.%) and a low  $\text{Al}_2\text{O}_3$  content.

Spinel in clinopyroxenite, gabbro and hornblende-bearing lithologies has variable  $\text{Al}_2\text{O}_3$  contents, and is very Ti–Fe-rich, but Cr-poor (Fig. 4d). This has to be anticipated for gabbroic and hornblende-rich rocks considering the evolved nature of their parental melts.

#### 4.3. Clinopyroxene a monitor of the evolution of the parental magma in Uralian–Alaskan-type complexes

One distinctive feature of the parental magma of Uralian–Alaskan-type complexes is the early and prevailing crystallization of clinopyroxene. It is present in all lithologies and, hence, the mineral is an ideal tracer for the evolution of the magma. Indeed the clinopyroxene composition monitors the course of crystallization by its systematic decrease of the  $\text{Mg}/(\text{Mg}+\text{Fe})$  with increasing  $\text{Al}_2\text{O}_3$ ,  $\text{TiO}_2$ , Mn or REE content from dunite, clinopyroxenite, and gabbro towards hornblende (Fig. 7). The strong decrease of Cr/(Cr+Al) in spinel from clinopyroxenite and gabbro (Table 3) can also be attributed to the crystallisation of diopside (Irvine, 1967). Fractional crystallization appears to be the dominant process controlling this chemical variation. However, several observations suggest that a more detailed and complex model is needed in order to explain, in particular, the trace element distribution in the clinopyroxene.

##### 4.3.1. Zonation of clinopyroxene — reaction with interstitial liquid

Clinopyroxene phenocrysts in some clinopyroxenite and gabbro samples (KT51, SB22, KT46) are zoned with regard to major and trace elements (Fig. 12). Although the differences for major elements are rather small, the cores of phenocrysts often have lower  $\text{Al}_2\text{O}_3$ , FeO, and higher  $\text{SiO}_2$  contents than their rims (Fig. 12a). However, there are large variations in incompatible trace elements. For example the rim can be enriched in REE by a factor of 1.5–2.5 compared to the core (Fig. 12b). In contrast concentrations of compatible elements, such as Cr, are higher in the core (Fig. 12a).

This zonation could reflect a magma mixing process. The crystal core formed in a magma chamber with relatively primitive liquid, rich in Cr but low in  $\text{Al}_2\text{O}_3$ ,  $\text{TiO}_2$ , and REE whereas the rim crystallized after the addition of a more fractionated melt.

Different La/Lu ratios in the core ( $\text{La}/\text{Lu} \sim 13$ ) and rim ( $\text{La}/\text{Lu} \sim 10$ ) of the phenocrysts from sample KT51 also suggest the existence of two different magmas. Interestingly, the chemical composition of interstitial clinopyroxene is similar to that of the phenocryst-rims (Table 4, KT51). This suggests that the interstitial clinopyroxene and the REE-rich clinopyroxene rims crystallized from fractionated residual melt in the pore space of the solidifying cumulate. This process may also explain the large variation of the REE concentration in clinopyroxene from a single lithology or even a single sample. For example, the Dy and Lu contents in clinopyroxene from

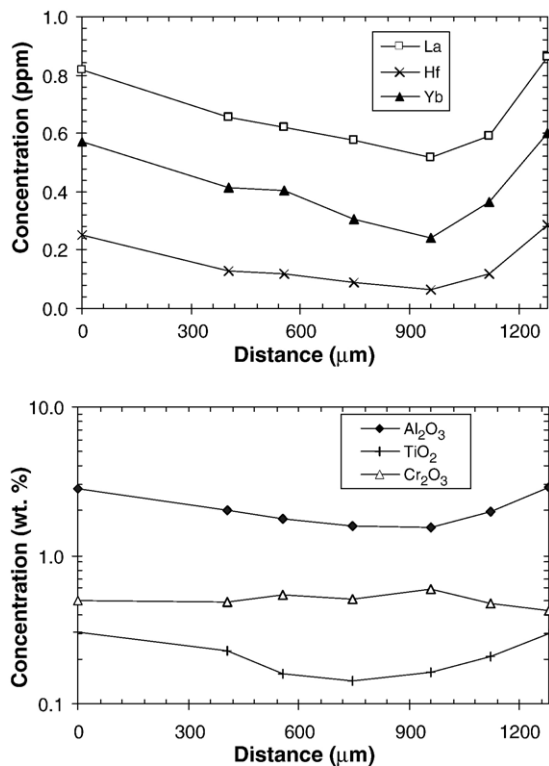


Fig. 12. Concentration profiles for a) major and b) trace elements in a diopside phenocryst from clinopyroxenite KT51.

dunites or clinopyroxenites can vary by more than a factor of 3 in one thin section (Fig. 9a).

#### 4.3.2. Clinopyroxene as monitor of the evolution of the parental magma

Presuming simple fractional crystallization the increased enrichment in REE concentrations in clinopyroxene from dunites compared to clinopyroxene from clinopyroxenites necessitates the parental magma to have been already more than 70% crystallized (F.C. in Fig. 9b). Such high degrees of crystallization are unrealistic. Even a crystal mush containing just 50% crystals would essentially behave like a solid due its high viscosity, and crystal separation would not be possible. Fractional crystallization of clinopyroxene also cannot explain the large fractionation of LREE from HREE that we observe overall in clinopyroxene from dunites and clinopyroxenites (La/Lu: 2–23; Fig. 9; Table 4). A pronounced enrichment and fractionation of REE can be achieved in a crystallizing and periodically tapped and replenished magma chamber (Shaw, 2006). Concentrations of compatible elements would become buffered at a certain level in such an open system magma chamber, due to the replenishment of more primitive magma

(Shaw, 2006). This could explain the rather low and constant NiO content in the MgO-rich olivine ( $Fo > 86$ ; NiO ~ 0.15 wt.%) from most dunites if compared to the trend defined by mantle-derived magmas (Fig. 3).

Two model calculations in Fig. 9b show the REE evolution of crystallizing clinopyroxene during such a process. The replenishing magma is assumed to have the same composition as the initial magma. In order to maximize the fractionation of LREE and HREE clinopyroxene is the only crystallizing phase (clinopyroxene/liquid partition coefficients are from Ionov et al. (1997).

In the one model (CER), 40% fractional crystallization is first followed by erupting 30% of the mass and the residual melt is mixed with the replenishing melt (30% of the initial magma mass). In the second model (CRE1, CER2) the cycle also starts with 40% of fractional crystallization. However, the residual liquid is replenished with 10% of the initial magma mass. Subsequently both magmas are mixed and 10% of the mass is erupted. The difference between these models is that CER is dominated by replenishment of the magma, whereas CRE is controlled by the crystallization process.

The CER model is characterized by a strong increase in the incompatible elements but little fractionation in the La/Lu ratio (Fig. 9b). Such a magma chamber system could explain the large Lu increase in some dunites and clinopyroxenites (SB22, KT37). However, most samples from Kytlym and Nizhnii Tagil display an increase in La/Lu as crystallization proceeds from dunite to clinopyroxenite (Fig. 9b). This is reflected in the CRE chamber in which cumulates display a continuous increase in REE accompanied by an enrichment of LREE relative to HREE (Fig. 9b). However, even such a model cannot explain the overall La/Lu variation in the dunite and clinopyroxenite cumulates of Kytlym. This necessitates the presence of parental magmas with different La/Lu ratios (model CRE1 and CRE2 in Fig. 9b).

It is appreciated that the proposed models are rather simplistic and represent only a few solutions out of numerous possibilities. The calculations can be tuned by adjusting the amount of fractional crystallization in between replenishment events and/or the amount of removed/added magma in order to better model specific details of the relationship between samples as well as between different intrusions. In fact it is reasonable to assume that during the life time of a magma chamber both CER and CRE processes will occur. This would explain most of the chemical variations we observe in the clinopyroxene.

An alternative explanation for the variable La/Lu ratios could be that parental magmas from different intrusions formed by variable degrees of partial melting.

However, given that the magmas are MgO-rich (MgO > 15 wt.%), the degree of partial melting would be rather high (> 10%), and hence, a strong fractionation of HREE from LREE is unlikely. Other possibilities would then have to be invoked, such as heterogeneous mantle sources variably enriched in highly incompatible elements or contamination of the parental magma with continental crust. Evaluation of such hypothesis is beyond the scope of this study.

#### 4.4. Implications for the formation of the chromitites

Chromitites occur as massive, but isolated lenses or schlieren in the dunites. The composition of the spinel in the dunite mirrors that in the chromitites. For example, the difference in Cr/(Cr+Al) observed between accessory spinel from dunites in Kytlym and Nizhnii Tagil is conserved in the associated chromitites (Fig. 11). This indicates that the formation of chromitites is due to the mobilization and re-precipitation of Cr in the dunite, probably during the final stages of crystallization. Recent studies comparing spinel compositions in chromitite with those in dunite and analyzing platinum-group minerals suggested that the chromitites formed by the interaction of a fluid with the dunite at temperatures of about 800–900 °C (Garuti et al., 1997; Chashchukhin et al., 2002; Garuti et al., 2003).

One intriguing observation is the extreme variation in the La/Lu ratio at rather low Lu concentrations in diopside from chromitites (KT31F, KT33; Fig. 9b). The diopside is strongly enriched in LREE compared to MREE and HREE resulting e.g. in high La/Lu of 20–60 compared to 5–15 in diopside from dunite and clinopyroxenite. Likewise, MREE are enriched relative to HREE (Fig. 9a). Some interstitial diopside from dunite samples close to chromitites (NT1, NT12) follow the same trends in Fig. 9. This suggests that the process, which formed the chromitite also crystallized or re-equilibrated the interstitial diopside in the neighbouring dunite.

The high La/Lu ratio at low and rather constant Lu concentrations cannot be explained by any crystallization process. Rather the steep trend built up by clinopyroxene from the chromitites and some dunites indicates a mixing relationship (MP-MC, Fig. 9b). One end member is represented by diopside with low REE contents and low La/Lu ratios. Its trace element pattern is similar to clinopyroxene which crystallized from the MgO-rich parental melt (Fig. 9b). The second end member is characterized by similar Lu concentrations but it has a La/Lu ratio greater than or equal to 60 (Fig. 9b). The origin of this component is enigmatic. Its chemical features are not preserved in any other rock type and there appears to be no

reasonable igneous hypothesis relating its composition to the parental melt or even to that of extreme fractionation products in interstitial spaces. However, one might speculate that it represents a hydrous fluid enriched in LREE which developed during the final crystallization of the pore liquid.

Diopside from clinopyroxenite veins in dunite (NT6, SB16, SB17) also have high La/Lu ratios comparable to those from chromitites. Again, clinopyroxene within a single sample displays variable La/Lu ratios and, typically, they define non-linear trends between La/Lu and Lu concentrations. This can also be observed in some clinopyroxenites (e.g. sample NT13, Fig. 9b). Such trends are characteristic of mixing relationships. This diopside can then be interpreted to represent the crystallization product from a mixture of the LREE-enriched “fluid” component (MC) and a fractionation product, maybe the residual interstitial liquid, of the parental ultramafic melt (MF, Fig. 9b). Therefore, we believe that there is a close genetic relationship between the diopside veins in dunite and the chromitites. These observations strengthen our earlier suggestion that the formation of the chromitites is a late stage magmatic process and thus an integral part of the evolution of the parental magma forming Uralian–Alaskan-type complexes.

#### 4.5. Trace element composition of the parental melt

Trace element abundances for the parental melt were calculated by dividing the average trace element content of the clinopyroxene in each sample by the diopside/liquid partition coefficient given by Ionov et al. (1997). Fig. 13 shows that trace element patterns for the parental melts are parallel regardless from which of the different main lithologies or even complexes they are calculated. The dunites from Kytlym (KT37) and Nizhnii Tagil (NT1) are derived from the most primitive parental melts having rather low REE concentrations of 1–10 times primitive mantle. The trace element concentrations in the parental melts systematically increase with increasing incompatibility but they also show pronounced negative anomalies for the HFSE.

The similarity of the trace elements in concentrations and patterns in all studied complexes implies that they were derived from parental melts with similar compositions and that these melts formed in source materials with similar trace element characteristics.

#### 4.6. Geotectonic setting

From major and trace element variations in minerals and whole rocks, a subduction related island arc setting

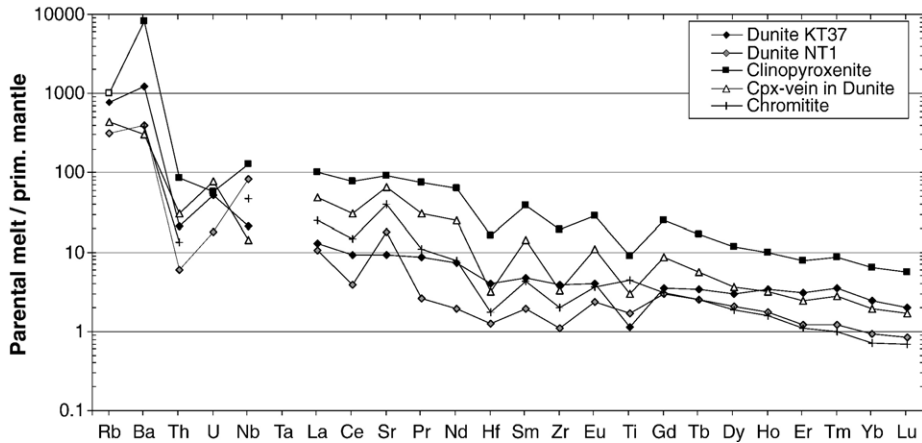


Fig. 13. Parental melt compositions calculated from trace element abundances in clinopyroxene. Partition coefficients are from Ionov et al. (1997).

has been assumed for the Uralian Platinum belt (Ivanov and Shmelev, 1996; Chashchukhin et al., 2002; Garuti et al., 2003) and for other belts of Uralian–Alaskan-type intrusions in Alaska/British Columbia and Kamchatka (e.g. Himmelberg and Loney, 1995; Batanova et al., 2005).

The trace element composition of the parental melts from the Uralian complexes are characterized by positive Sr and negative anomalies of the HFSE (Fig. 13). This supports the idea that these rocks have a subduction related origin. Clinopyroxene compositions can also be used to discriminate between different geotectonic settings. Fig. 14 shows the percentage of tetrahedral sites occupied by Al vs. the  $\text{TiO}_2$  content (Loucks, 1990). Our data are in good agreement with clinopyroxene compositions from other occurrences in the Ural Mountains and with Uralian–Alaskan-type complexes world wide. They clearly follow the trend defined by volcanic rocks and cumulates from island arc magmas (Loucks, 1990; Himmelberg and Loney, 1995) which is significantly steeper than that observed for plutonic and volcanic rocks related to continental rifts or large igneous provinces. At low  $\text{Al}^{\text{IV}}$  and  $\text{TiO}_2$  concentrations, the island-arc and MORB-trends are similar. However the enriched trace element pattern in the parental magma from the Ural Mountains clearly distinguishes them from MORB-magmas.

#### 4.7. Parental magmas of Uralian–Alaskan-type complexes: comparison with ankaramites

The trace element composition for melts determined in this study is similar to that calculated by Batanova et al. (2005) using melt inclusion data from the Galmoenan Uralian–Alaskan-type complex in Kamchatka. The coincidence with whole rock data from zoned mafic–

ultramafic complexes in Alaska and British Columbia (Himmelberg and Loney, 1995), indicates that this class of intrusions formed under similar physico-chemical conditions and in mantle sources with comparable compositional fingerprints. However, the petrological affiliation of Uralian–Alaskan-type complexes to specific mantle-derived melts is not well established.

Irvine (1973) proposed that there is a genetic relationship between ankaramitic dykes in British Columbia and the ultramafic Uralian–Alaskan-type intrusions of the

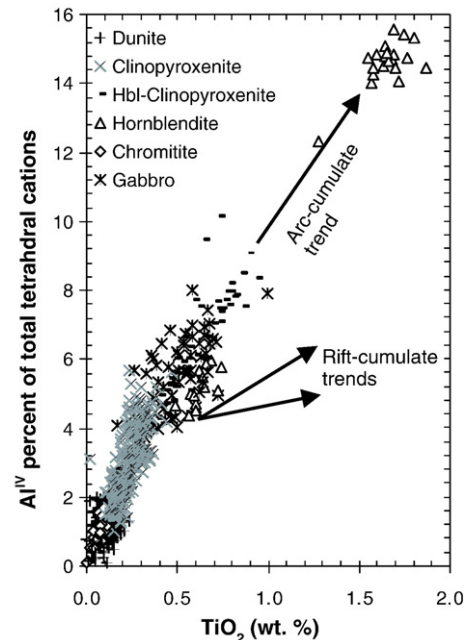


Fig. 14.  $\text{Al}^{\text{IV}}$  (in percent of total tetrahedral cations) vs.  $\text{TiO}_2$  content in clinopyroxene. Trends are shown for cumulates and volcanic rocks from different tectonic settings. Data is from Loucks (1990).

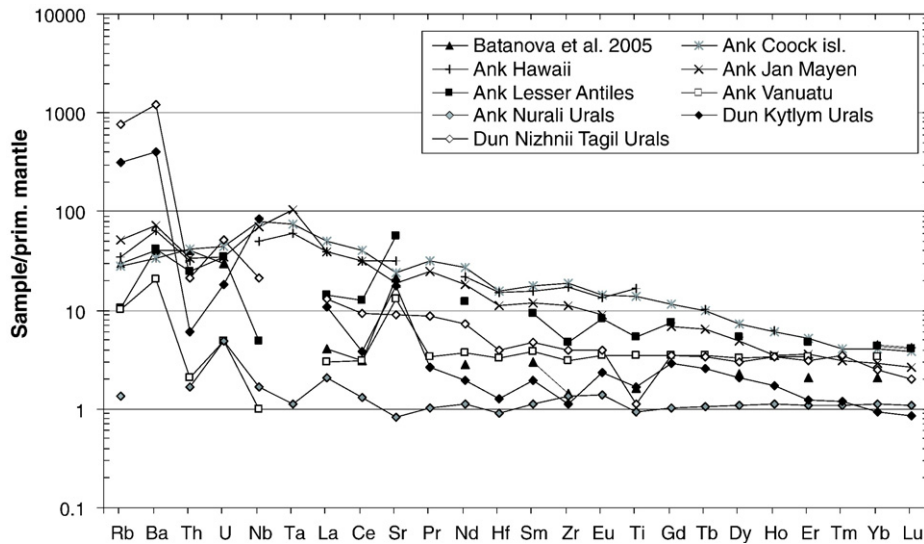


Fig. 15. Comparison of trace element abundances in Ankaramites (Ank) from different locations compared with those from the parental melt as proposed by [Batanova et al. \(2005\)](#) and calculated in this study from clinopyroxene from the most primitive dunite (Dun) in Nizhni Tagil and Kytlym. For references see text.

Cordillera of Alaska and British Columbia. Ankaramites are known from different geotectonic settings e.g. ocean islands ([Frey et al., 1991](#); [Woodhead, 1996](#); [Tronnes et al., 1999](#)) and island-arcs ([Barsdell and Smith, 1989](#); [Barsdell, 1989](#); [Thirlwall et al., 1994](#); [Mossman et al., 2000](#)). They represent a class of clinopyroxene-rich, mafic–ultramafic volcanic rocks that share many chemical and mineralogical features with Uralian–Alaskan-type mafic to ultramafic intrusions. These volcanic rocks are characterized by the early crystallization of olivine, spinel and clinopyroxene. Therefore, the subvolcanic emplacement and crystallization of such melts should result in the formation of dunitic, wehrlitic and clinopyroxenic cumulates containing accessory spinel, as observed in Uralian–Alaskan-type intrusions.

The chemical composition of chromian spinel phenocrysts in ankaramites from different localities (Vanuatu Arc, Pacific Ocean, Greenhills complex, New Zealand, Cameroon) ([Barsdell and Smith, 1989](#); [Barsdell, 1989](#); [Nono et al., 1994](#); [Mossman et al., 2000](#)) is similar to that for spinel from the studied complexes in the Ural Mountains ([Fig. 4f](#)). Some ankaramites appear to be derived from more primitive melts as their spinel is richer in Cr than observed for the Uralian complexes.

Trace element patterns from subduction-related ankaramites from Vanuatu in the Pacific Ocean ([Barsdell, 1989](#)) and the Lesser Antilles ([Thirlwall et al., 1994](#)) are in good agreement with our calculated melt compositions ([Fig. 15](#)). They share the negative anomalies for Hf, Zr and Ti, the positive Sr anomaly, and the LREE-enrichment relative to the HREE.

These features are also observed in ankaramites intruding the Nurali Massive, which is located close to the Uralian–Alaskan-type complexes in the Tagil–Magnitogorsk zone ([Spadea et al., 2002](#)). These authors suggested that they are related to island arc magmatism in the Magnitogorsk arc. Age, geochemical and spatial relationships may even imply a genetic link between these ankaramites and the Uralian–Alaskan-type complexes of the UPB. Hence in summarizing these observations we agree with the suggestion by [Irvine \(1973\)](#) that ankaramites could represent the parental magmas of Uralian–Alaskan-type complexes.

## 5. Conclusions

This study describes Uralian–Alaskan-type complexes from the Ural Platinum Belt in the Ural Mountains. It constrains the composition of the parental magma by monitoring the evolution of the complexes using mainly major and trace element abundances of spinel, olvine and clinopyroxene.

The complexes in the Ural Mountains share many distinct structural, petrological and geochemical features described from other examples world wide. The Uralian complexes are interpreted to represent cumulates from an ankaramitic ultramafic melt which successively crystallized olivine+chromite, olivine+chromite+clinopyroxene, clinopyroxene+chromian magnetite, and eventually clinopyroxene+spinel+plagioclase+phlogopite±K-feldspar±nepheline resulting in dunites, wehrlites, clinopyroxenites and gabbros, respectively.

The early stages of crystallization are monitored by a decreasing Fo content in the olivine and a decreasing Cr/(Cr+Al) in the coexisting chromite. The high Fo content of olivine (Fo>90) and the high Cr/(Cr+Al) in the spinel (Cr/(Cr+Al)~080) imply a parental magma rich in MgO (>15 wt.%) but poor in Al<sub>2</sub>O<sub>3</sub>. The positive anomaly in Sr, negative anomalies in HFSE, and the high ratio of the tetrahedrally coordinated Al to the TiO<sub>2</sub> content in clinopyroxene indicate that these rocks crystallized from magmas forming at destructive plate margins. Irvine (1973) proposed a genetic relationship between Uralian–Alaskan-type complexes and ankaramites. The good agreement between the major and trace element composition of accessory and rock forming minerals from Uralian–Alaskan-type complexes in the Urals with those of subduction-related ankaramites from different localities world wide support Irvine's suggestion.

Nevertheless, the compositions of minerals in different complexes from the Ural Mountains display small but significant differences in the parental melt compositions. For example, spinel and olivine from Kytlym tend to be more Al<sub>2</sub>O<sub>3</sub> and fayalite rich, respectively, than those from Nizhnii Tagil. In addition, clinopyroxene from different complexes and lithologies could display large variations in their LREE/HREE ratios. Different stages of evolution of the parental magma at the time of emplacement can explain these differences. However, this could also be due to crustal contamination processes, or caused by different degrees of partial melting in a heterogeneous mantle source.

The dominance of dunite and clinopyroxenite in the complexes necessitates an extensive and prolonged crystallization of olivine and clinopyroxene. This could be achieved during the crystallization of a continuously erupted and replenished magma chamber. Such a model is also required in order to explain the strong enrichment of incompatible trace elements as the crystallization of olivine and clinopyroxene proceeds.

Clinopyroxenites and gabbros have zoned clinopyroxene phenocrysts which probably indicate magmatic reactions between a high-temperature clinopyroxene and a crystallizing interstitial liquid during the later stages of the evolution of the cumulate pile. The local replacement of clinopyroxene with hornblende in the clinopyroxenites from Svetley Bor also demonstrates the presence of a hydrous melt or fluid during the final stages of solidification.

Diopside from chromitites and cross cutting diopside veins in dunite share similar trace element patterns with LREE/HREE ratios higher than those in diopside from all other lithologies. It implies the involvement of a fluid

or melt during the formation of the chromitites, which is more enriched in highly incompatible elements than the parental magma. The chromitites likely formed at high temperatures (800–900 °C) during the waning stages of crystallization. However, there is little information on the mechanism responsible for the mobilization of Cr and PGE in the dunites or their ultimate concentration in the chromitite lenses.

Ongoing investigations of the Os isotope systematics and the distribution of the platinum group elements would provide additional constraints on the formation of the PGE-rich chromitite bodies. It could also strengthen the proposed genetic relationships between the different lithologies as well as between ankaramites and Uralian–Alaskan-type complexes.

### Acknowledgement

We thank N. Groschopf, K Herwig, B. Stoll and B. Schulz-Dobrick for the assistance during the LA-ICPMS and Microprobe analyses. D. Harlov and an anonymous reviewer are thanked for their helpful suggestions that significantly improved the manuscript. This Study was funded by grant GK392 of the Graduiertenkolleg 'Stoffbestand und Entwicklung von Kruste und Mantel' at the University of Mainz to J. Krause.

### Appendix A. Supplementary data

Supplementary data associated with this article can be found, in the online version, at doi:10.1016/j.lithos.2006.07.018.

### References

- Barnes, S.J., Roeder, P.L., 2001. The range of spinel compositions in terrestrial mafic and ultramafic rocks. *Journal of Petrology* 42 (12), 2279–2302.
- Barsdell, M., 1989. Petrology and petrogenesis of Clinopyroxene-rich tholeiitic lavas, Merelava volcano, Vanuatu. *Journal of Petrology* 29 (5), 927–964.
- Barsdell, M., Smith, I.E.M., 1989. Petrology of recrystallized ultramafic xenoliths from Merelava volcano, Vanuatu. *Contributions to Mineralogy and Petrology* 102, 230–241.
- Batanova, V.G., Astrakhantsev, O.V., 1992. Tectonic position and origins of the zoned mafic–ultramafic plutons in the Northern Olyutor Zone, Koryak Highlands. *Geotectonics* 26 (2), 153–165.
- Batanova, V.G., Astrakhantsev, O.V., 1994. Island-arc mafic–ultramafic plutonic complexes of northern Kamchatka. In: Ishiwatari, A., Malpas, J., Ishizuka, H. (Eds.), *Proceedings of the 29th International Geological Congress, Part D, Circum-Pacific-ophiolites VSP*, pp. 129–143.
- Batanova, V.G., Pertsev, A.N., Kamenetsky, V.S., Ariskin, A.A., Mochalov, A.G., Sobolev, A.V., 2005. Crustal evolution of island-arc ultramafic magma: Galmoenan pyroxenites–dunite plutonic

- complex, Koryak Highland (Far East Russia). *Journal of Petrology* 46, 1345–1366.
- Bédard, J.H., 2001. Parental magmas of the Nain Plutonic Suite anorthositic and mafic cumulates: a trace element modelling approach. *Contributions to Mineralogy and Petrology* 141, 747–771.
- Chashchukhin, I.S., Votyakov, S.L., Pushkarev, E.V., Anikina, E., 2002. Oxithermobarometry of ultramafic rocks from the Ural Platinum Belt. *Geochemistry International* 40 (8), 762–778.
- Clark, T., 1980. Petrology of the Turnagain ultramafic complex, northwestern British Columbia. *Canadian Journal of Earth Sciences* 17, 744–757.
- Cookerbo, H.O., Bustin, R.M., Wilks, K.R., 1997. Detrital chromian spinel compositions used to reconstruct the tectonic setting or provenance: implications for orogeny in the Canadian Cordillera. *Journal of Sedimentary Research* 67 (1), 116–123.
- Findlay, D.C., 1969. Origin of the Tulameen ultramafic-gabbro complex, southern British Columbia. *Canadian Journal of Earth Sciences* 6, 399–425.
- Frey, F.A., Garcia, M.O., Wise, W.S., Kennedy, A.K., Gurriet, P., Albarède, F., 1991. The evolution of Mauna Kea volcano, Hawaii: petrogenesis of tholeiitic and alkalic basalts. *Journal of Geophysical Research* B96, 14347–14375.
- Garuti, G., Fershtater, G., Bea, F., Montero, P., Pushkarev, E.V., Zaccarini, F., 1997. Platinum-group elements as petrological indicators in mafic–ultramafic intrusions of the central and southern Urals: preliminary results. *Tectonophysics* 276, 181–194.
- Garuti, G., Pushkarev, E.V., Zaccarini, F., Cabella, R., Anikina, E., 2003. Chromite composition and platinum-group mineral assemblage in the Uktus Uralian–Alaskan-type complex (Central Urals, Russia). *Mineralium Deposita* 38, 312–326.
- Hart, S.R., Dunn, T., 1993. Experimental cpx/melt partitioning of 24 trace elements. *Contributions to Mineralogy and Petrology* 113, 1–8.
- Hill, R., Roeder, P., 1974. The crystallization of spinel from basaltic liquid as a function of oxygen fugacity. *Journal of Geology* 82, 709–729.
- Himmelberg, R.G., Loney, R.A., 1995. Characteristics and petrogenesis of Alaskan-Type ultramafic–mafic intrusions, southeastern Alaska. *US Geological Survey Professional Paper* 1564, 1–47.
- Himmelberg, R.G., Loney, R.A., Craig, J.T., 1986. Petrogenesis of the ultramafic complex at the Blashke Islands, southeastern Alaska. *US Geological Survey Bulletin* 1662, 1–14.
- Hofmann, A.W., 1988. Chemical differentiation on the earth: the relationship between mantle, continental crust, and oceanic crust. *Earth and Planetary Science Letters* 90, 297–314.
- Ionov, D.A., Griffin, W.L., O'Reilly, S.Y., 1997. Volatile-bearing minerals and lithophile trace elements in the upper mantle. *Chemical Geology* 141, 153–184.
- Ionov, D.A., Bodinier, J.-L., Mukasa, S.B., Zanetti, A., 2002. Mechanisms and sources of mantle metasomatism: major and trace element compositions of peridotite xenoliths from Spitzbergen in the context of numerical modelling. *Journal of Petrology* 43 (12), 2219–2259.
- Irvine, T.N., 1967. Chromian spinel as a petrogenetic indicator; Part 2, Petrologic applications. *Canadian Journal of Earth Sciences* 7, 71–103.
- Irvine, T.N., 1973. Bridget Cove volcanics, Juneau Area, Alaska: possible parental magma of Alaskan-type ultramafic complexes. *Carnegie Institution Washington Yearbook*, vol. 72, pp. 478–491.
- Ivanov, K.S., Shmelev, V.R., 1996. Urals Platinum Belt — magmatic trace of an early Paleozoic subduction zone. *Doklady Rossijskoj Akademii Nauk*. A 347 (5), 649–652.
- Jackson, E.D., 1969. Chemical variation in coexisting chromite and olivine in chromitite zones of the Stillwater Complex. In: Wilson, H.D.B. (Ed.), *Magmatic Ore Deposits a Symposium*. Economic Geology, Monograph, vol. 4, pp. 41–71.
- Jochum, K.P., Stoll, B., Herwig, K., Amini, M. submitted for publication. Trace element and isotope analysis of geo- and cosmochemical samples by laser ablation sector field ICP-MS. In: Douthitt, C.B. (ed.), *High resolution ICP-MS*.
- Lee, Y.L., 1999. Geotectonic significance of detrital chromian spinel: a review. *Geosciences Journal* 3 (1), 23–29.
- Lehmann, J., 1983. Diffusion between olivine and spinel: application to geothermometry. *Earth and Planetary Science Letters* 64, 123–138.
- Loucks, R.B., 1990. Discrimination of ophiolitic from nonophiolitic ultramafic–mafic allochthons in orogenic belts by the Al/Ti ratio in Clinopyroxene. *Geology* 18, 346–349.
- McKenzie, D., O'Nions, R.K., 1991. Partial melt distributions from inversion of rare earth element concentrations. *Journal of Petrology* 32 (5), 1021–1091.
- Melcher, F., Grum, W., Simon, G., Thalhammer, T., Stumpf, E., 1997. Petrogenesis of the ophiolitic giant chromitite deposits of Kempirsai, Kazakhstan: a study of solid and fluid inclusions in chromite. *Journal of Petrology* 40 (10), 1419–1458.
- Mossman, D.J., Coombs, D.S., Kawachi, Y., Reay, A., 2000. High-Mg Arc-ankaramitic dikes, Greenhills complex, Southland, New Zealand. *Canadian Mineralogist* 38, 191–216.
- Nixon, G.T., Hammack, J.L., Connelly, J.N., Case, G., Paterson, W.P.E., 1990. Geology and noble metal geochemistry of the Polariss ultramafic complex, north-central British Columbia. *Geologic fieldwork 1989: British Columbia Ministry of Energy, Mines and Petroleum resources*, vol. 1988, 1, pp. 307–404.
- Noble, J.A., Taylor, H.P., 1960. Correlation of the ultramafic complexes of southeastern Alaska with those of North America and the World. 21st International Geological Congress in Copenhagen 1960. Report part 13, pp. 188–197.
- Nono, A., Déruelle, B., Demaiffe, D., Kambou, R., 1994. *Journal of Volcanology and Geothermal Research* 60, 147–178.
- Roeder, P.L., 1994. Chromite: from the fiery rain of chondrules to the Kilauea Iki lava lake. *Canadian Mineralogist* 32, 729–746.
- Sack, R.O., Ghiorso, M.S., 1991a. Chromite as a petrogenetic indicator. In: Lindsley (Ed.), *Oxide Minerals Petrogenetic and Magnetic Significance*. *Reviews in Mineralogy*, vol. 25, pp. 323–353.
- Sack, R.O., Ghiorso, M.S., 1991b. Chromian spinel as petrogenetic indicators: thermodynamics and petrological applications. *American Mineralogist* 76, 827–847.
- Savelieva, G.N., Pertsev, A.N., Astrakhantsev, O.V., Denisova, E.A., Boudier, F., Bosch, D., Puchkova, A.V., 1999. Kytlym pluton, north Urals: structure and emplacement history. *Geotectonics* 33 (2), 119–142.
- Savelieva, G.N., Sharaskin, A.Y., Saveliev, A.A., Spadea, P., Pertsev, A.N., Babarina, I.I., 2002. Ophiolites and zoned mafic–ultramafic massifs of the Urals: a comparative analysis and some tectonic implications. In: Browen, D., Juhlin, C., Puchkov, V. (Eds.), *Mountain building in the Uralides: Pangea to the present*. *Geophysical Monograph*, vol. 132, pp. 135–153.
- Shaw, D.M., 2006. *Trace Elements in Magmas A Theoretical Treatment*. Cambridge University, pp. 1–243.
- Spadea, P., D'Antonio, M., Kosarev, A., Gorozhanina, Y., Brown, D., 2002. Arc-continent collision in the southern Urals: petrogenetic aspects of the forearc–arc complex. In: Browen, D., Juhlin, C., Puchkov, V. (Eds.), *Mountainbuilding in the Uralides: Pangea to the Present*. *Geophysical Monograph*, vol. 132, pp. 101–134.

- Tamura, A., Arai, S., 2005. Unmixed spinel in chromitite from the Iwanai–Dake peridotite complex, Hokkaido, Japan: a reaction between peridotite and highly oxidized magma in the mantle wedge. *American Mineralogist* 90, 473–480.
- Taylor, H.P., 1967. The zoned ultramafic complexes of southeastern Alaska, part 4.III. In: Wyllie, P.J. (Ed.), *Ultramafic and Related Rocks*. John Wiley, New York, pp. 96–118.
- Taylor, H.P., Noble, J.A., 1960. Origin of the ultramafic complexes in southeastern Alaska. 21st International Geological Congress in Copenhagen 1960. Report part 13, pp. 175–187.
- Thirlwall, M.F., Smith, T.E., Graham, A.M., Theodorou, N., Hollings, P., Davidson, J.P., Arculus, R.J., 1994. High field strength element anomalies in arc lavas: source or process? *Journal of Petrology* 35, 819–838.
- Tronnes, R.G., Planke, S., Sundvoll, B., Imsland, P., 1999. Recent volcanic rocks from Jan Mayen: low-degree melt fractions of enriched northeast Atlantic mantle. *Journal of Geophysical Research* 104 (B4), 7153–7168.
- Van der Veen, A.H., Maaskant, P., 1995. Chromian spinel mineralogy of the Staré Ransko gabbro-peridotite, Czech Republic, and its implications for sulfide mineralization. *Mineralium Deposita* 30, 397–407.
- Woodhead, J.D., 1996. Extreme HIMU in an oceanic setting: the geochemistry of Mangaia Island (Polynesia), and temporal evolution of the Cook-Austral Hot Spot. *Journal of Volcanology and Geothermal Research* 72, 1–19.
- Wyllie, P.J., 1967. *Ultramafic and Related Rocks*. John Wiley, New York, pp. 1–464.
- Zhou, M.-F., Lightfoot, P.C., Keays, R.R., Moore, M.L., Morrison, G.G., 1997. Petrogenetic significance of chromian spinels from the Sudbury Igneous Complex, Ontario, Canada. *Canadian Journal of Earth Sciences* 34, 1405–1419.